2-in-1 Smart Panels:

Multifunctional Structures with Embedded Patch Antennas

by

Valorie Platero

A Thesis

submitted to the University of Manitoba

in fulfillment of the thesis requirement for the degree of

Master of Science

in

Mechanical Engineering

Winnipeg, Manitoba, Canada

Abstract

This thesis evaluates the feasibility of an embedded antenna multifunctional structure (MFS) for spacecraft applications. The increasing commercialization and miniaturization of space missions call for versatile subsystems that make efficient use of limited spacecraft volumes. This research investigates a design for a microstrip patch antenna with an SU-8 photoresist substrate on a hybrid composite structural panel comprised of aluminum, carbon fibre composite (CFC) and polyethylene fibre composite (PFC) materials. While the proposed design does not outperform high-powered antennas such as reflectors, they can be utilized as secondary communication antennas for tracking, telelemetry and command (TT&C).

In order to design and model the antenna in ANSYS HFSS electromagnetic simulations, all of the materials are characterized first. I performed a series of tests using parallel plate and microstrip devices to extract their electrical properties. After modelling and design, a manufacturing process for the substrate is optimized to work around the thermal constraints of the composite materials. The antenna is then deposited on top using a stencil and copper deposition methods.

During the connector attachment process, the antenna prototype was subjected to rapid temperature changes which caused the SU-8 substrate layer and copper patch to crack in several places. The cracking introduced air gaps between the substrate and aluminum ground plane, and the microstrip patch was ammended by placing copper tape on top. After such repairs, the antenna prototype is then measured at an operational frequency of 2.5 GHz, with a -10 dB bandwidth of 60 MHz, and a peak gain of 1.45 dB. These results were followed by an investigation of various loss mechanisms. Although the resulting performance of the MFS antenna did not meet the expectations and criteria, there are still potential applications with my recommendations for future work in this research area that can improve the feasibility of this technology.

Acknowledgements

I would like to acknowledge and thank everyone who supported me throughout my journey. This has been the most challenging undertaking of my academic career and I appreciate everyone helping me get to the end of this long and winding road.

Firstly, I would like to thank my advisors, Dr. Philip Ferguson and Dr. Dustin Isleifson, for their inspiration and guidance throughout my research. Even through roadblocks, I am thankful for your patience and helping me push through to the end. Space is hard, but you make it look easy.

Secondly, I'd like to thank Dr. Raghavan Jayaraman and Dr. Adebayo Emmanuel from the University of Manitoba's Composite Materials and Structures Research Group (CMSRG), Dr. Cyrus Shafai, Shirin Ramezanzadehyazdi, and Dwayne Chrusch from the Nano-Systems Fabrication Laboratory (NSFL), Brendan Pachal from the University of Manitoba Space Technology and Advanced Research Lab (STAR Lab), and Ehsan Zeynali from the University of Manitoba Antennas Laboratory. I'd also like to thank my friends and labmates from STAR Lab for making my graduate years much more enjoyable.

Next, I'd like to thank the Natural Sciences and Engineering Research Council (NSERC) / Magellan Aerospace Industrial Research Chair in Satellite Engineering for funding this research.

Finally, I'd like to thank my friends and family, and especially my parents Ramon and Vivian, who uprooted their lives when we immigrated to Canada. I will always be grateful for your unconditional love and support and I wouldn't be where I am now without you. I dedicate this thesis to you.

Contents

List of Figures

List of Tables

Nomenclature

CFC	Carbon Fibre Composites
CFRP	Carbon Fibre Reinforced Polymer
COTS	Commercial Off-the-Shelf
DUT	Device Under Test
HDPE	High Density Polyethylene
LDPE	Low Density Polyethylene
NASA	National Aeronautics and Space Administration
MMOD	Micrometeoroid Orbital Debris
MFS	Multifunctional Structures
PFC	Polyethylene Fibre Composite
PVD	Physical Vapour Deposition
RF	Radio Frequency
S_{11}	Reflection Coefficient
S_{21}	Transmission Coefficient
SAR	Synthetic Aperture Radar
TT&C	Telemetry, Tracking and Command
UHMWPE	Ultra-high molecular weight polyethylene
UV	Ultraviolet
VNA	Vector Network Analyzer

Chapter 1

Introduction

1.1 Overview

Historically, government agencies were the first to venture out into space and the subsequent development was managed by bodies like NASA or ESA with established contractors. As space mission goals become more ambitious, the demand in functionalities of spacecraft increase in complexity and cost [1–3]. The advent of space commercialization allowed for the space community to grow by including groups outside of major agencies. Increased accessibility provides the opportunity for these groups to manage and operate spacecraft almost independently from mission concept design to launch [4]. Accessibility and commercialization drive the advancement of technologies that improve cost and performance efficiency such as:

- Multifunctional structures (MFS)
- Composite materials
- Spacecraft miniaturization
- Microstrip antennas

An amalgamation of these technologies is studied in this thesis, which explores the feasibility of embedding microstrip antennas in composite materials to create a multifunctional structure that facilitates

spacecraft miniaturization. The proposed component is a "smart panel" that functions as the satellite structure and communications antenna that operates in the S-band. The respective advantages of each of the aforementioned technologies are as follows:

1) Volume Efficiency: MFS integrate spacecraft bus functionalities within the structure and make efficient use of space by utilizing otherwise passive elements. This method reduces mass and maximizes usable volume for other instruments and payloads, adding value to the mission.

2) Reduced Mass: Composite materials possess the desired structural qualities of traditional materials such as metals, while reducing weight significantly [5]. Although carbon fiber composites (CFC) are common in the aviation industry, they are only recently being adopted for space flight on a limited basis [6,7].

3) Improved Access to Space: Miniaturized spacecraft bring down the barrier of entry for testing new technologies or conducting scientific investigations [8,9]. By minimizing the cost and safety-critical nature of the spacecraft, there is less risk involved in adopting the most cutting-edge advances in research.

4) Ease of Integration: Microstrip antennas have thin planar profiles and are easily fabricated [10], therefore integration with the structure can create versatile systems. Implementing planar antennas reduces collision and non-deployment risks. Antennas that provide a delicate balance of gain performance with minimized component footprint can make communications systems more effective.

5) Adaptable Communications Solutions: A challenging element of space missions can be the communications system, which is responsible for transmitting critical data over vast distances despite limitations on available power and space. A multifunctional antenna structure that can be adapted in size has potential applications for both large and small satellites. Larger spacecraft lend more surface area that

increase aperture size for more demanding data requirements, and small ones are able to work around their stricter limitations with less demanding requirements. While miniaturized spacecraft constraints are given special consideration in the evaluation of the component, the design allows for both use cases.

1.2 Hypotheses

The objective of this research is to develop a smart panel that can transmit and receive communication signals while maintaining structural integrity to support the spacecraft. The methods and tests discussed in this thesis are performed to verify the following hypotheses:

1. Microstrip antennas can be successfully deposited onto composite materials
2. Carbon fibre reinforced polymers (CFRP) can be incorporated into the smart panel without detriment to antenna performance
3. The embedded antenna will meet the performance standards for satellite communications
4. The smart panel reduces the component footprint and maximizes useable spacecraft volume

1.3 Challenges

Some of the challenges involved with this research include electrical characterization of materials, manufacturing feasibility, and patch antenna limitations. The most significant challenge to the design and implementation of MFS is the merging of mechanical and electrical functionalities. Developments in each subsystem are usually done separately and integrated towards the later phases of the mission. With MFS, the design inherently takes both systems into account and developed jointly so they can be hybridized without detriment to their individual performance.

An aspect of electrical design that is not normally investigated during mechanical structure design is the electrical properties of materials such as conductivity and permittivity. While heat conductivity is useful for the structure's thermal distribution and control, electrical conductivity can react with the emission field

of the antenna radiation. This can be addressed by the antenna design and utilized as a ground plane. In order to properly take advantage of this, the materials of which the structural antenna is comprised must be characterized. Afterwards, the geometry and stack lay-up of the panel must be accurately represented in models for the design and simulation of the antenna panel.

Another challenge of this research is the feasibility of a streamlined assembly process of the smart structure technology. In order for the component to prove cost efficiency, it must demonstrate adaptable manufacturability and reduced integration overhead. The bonding of an antenna substrate onto the composite material and the copper deposition method have to take into account constraints such as temperature limitations. The substrate material itself requires the ability for adhesion to any size and shape of the ground plane, and still maintain desirable permittivity and loss tangent properties.

While microstrip antennas have the advantages of cheap and easy fabrication, there are some drawbacks that affect the potential use cases. Rectangular patch antennas typically operate on a narrow bandwidth (2%-5% [10]) which limits the data rate of satellite communications. CubeSat data rates are normally within the range of 1.2 - 9.6 kbit/s [16], which is still achievable with the patch antenna's bandwidth, but restricts high-volume data such as mapping and high resolution images. The potentially high directivity of patch antennas can be seen as an advantage for more focused beams and power efficiency, but it might also impose higher pointing accuracy requirements on the spacecraft depending on the nature of the mission. Two possible solutions include placing multiple antennas on at least four faces of the spacecraft to create a pseudo-omnidirectional pattern, or implementing beam steering capabilities using phased arrays. Although they have minimal volumes, they also take up significant surface areas. Mounting patch antennas on the outside face of satellites occupies space that could otherwise be used by instruments such as solar panels and camera lenses.

1.4 Contributions

The work presented in this thesis develops a design of a multifunctional antenna structure that jointly fulfills the roles of a mechanical support structure and a radiating communications component. The antenna is designed to comply with increased gain and beam steering requirements imposed by the CubeSat applications in Section 2.6. Here is a summary of my research contributions:

- Utilization and characterization of hybrid composite materials and SU-8 photoresist
- Analysis of SU-8 photoresist as an antenna dielectric substrate
- Novel manufacturing method for a MFS antenna device
- Design of a versatile component with reduced micrometeoroid orbital debris (MMOD) and non-deployment risk
- Spatial and cost efficiency for satellite missions

The antenna design takes a novel approach of building on top of a pre-existing hybrid composite radiation shielding design by Emmanuel [17], comprised of polyethylene fibre composite (PFC), carbon fibre composite (CFC), and aluminum. The composite face is utilized as the antenna ground plane, SU-8 photoresist is deposited as the substrate, followed by the sputtering of a thin copper layer as the patch antenna and feed network. Advantages contributed by this design include the manufacturing process, its adaptable functionality, cost-effectiveness, and increased system reliability through reduced collision and non-deployment risks.

The manufacturing process of this design is improved by the characteristics of SU-8. The material starts out as a liquid and is poured over the ground plane allowing for versatile deposition. Solidification of the SU-8 eliminates the need for adhesives or fasteners between the substrate and ground plane. Finally, copper sputtering of the radiative elements enable the realization of more complex microstrip designs for enhanced feeding networks and geometries.

Setting CubeSat constraints on the design creates an antenna component that is compliant with the standardization philosophy of the platform. While parameters such as operational frequency and size adhere to these standards, features such as gain and beam forming have been enhanced. A building block approach based on the "U"-unit can be taken in order to construct larger arrays if needed. This makes it a good candidate for outsourcing to a commercial off-the-shelf (COTS) solution, which is a beneficial practice amongst CubeSat teams.

The component overlap created by the MFS combination helps reduce overhead and verification activities required to qualify two separate systems, and therefore, reduces cost. In addition, structural components are built and rigorously tested for the harsh space environment, which increases component reliability. The fusion of both systems brings forth new constraints and challenges, but ultimately result in a more resilient component. Extended testing scope, reduced risks from MMOD and non-deployment, and added radiation shielding forge a component with enhanced reliability. Bolstering a component's reliability can increase the chances of being chosen for flight and achieving heritage.

This research has advanced the field of antennas as MFS by innovating a novel and different technique to embedding antennas than the existing technologies reviewed in Chapter 2. The performance of SU-8 as a substrate compounded with a hybrid composite ground plane for satellite antenna applications have not been previously explored. Data gathered in the characterization of chosen materials are also valuable to future works aiming to expand this concept.

1.5 Outline

Chapter 2 provides an in-depth background and literature review on the different fields involved with the research. This review consists of different topics about antennas, microstrip devices, large and small spacecraft, and multifunctional structures.

Chapter 3 introduces the different materials chosen to create the multifunctional antenna structure. The

methods of analysis, procedures, and test equipment to characterize these materials are discussed. Electrical properties such as conductivity, permittivity, and loss tangent are measured and evaluated for their eligibility for MFS and space applications.

Chapter 4 presents some use case studies on the potential applications of the proposed MFS antenna. The data gathered from Chapter 3 is then used to design the patch antenna system. The electrical properties and dimensions obtained are input into an ANSYS HFSS model and simulated. The radiation performance of the array and beam steering capability is evaluated through realized gain, half power beamwidth, return loss and bandwidth.

Chapter 5 describes the process of manufacturing the proposed MFS antenna design. The laboratory procedures and equipment used to create the antenna are discussed. Practical considerations such as manufacturing tolerances and sources of loss are examined.

Chapter 6 presents the results of antenna radiation performance of the constructed MFS in an anechoic chamber. The theoretical versus measured characteristics of the antenna are compared to the expectations from Chapter 4, and discrepancies are analyzed for possible causes.

Chapter 7 is the summary of this journey and the conclusions of my research contributions.

Chapter 2

Background

2.1 Spacecraft Antennas

There is a vast range of communications requirements for different spacecraft that are unique to the mission. These characteristics include data volume and rate, frequency of operation, service area, and signal-to-noise ratio. The main types of antennas used are wide, earth, and narrow coverage [18]. The function and type of data will dictate which antennas are required, each with their advantages and disadvantages.

Wide coverage or omnidirectional antennas are required for telemetry, tracking, and command (TT&C) applications. TT&C data help satellite operators monitor bus health, track its location, and send commands to the on-board computer. These types of transmissions use lower data rates and frequencies but require wide coverage so it can be accessed regardless of the satellite's orientation [18]. This type of antenna is also useful for spacecraft with a low pointing accuracy. Omnidirectional antennas have uniform and 360°coverage in one plane, and includes dipoles, loops, and broadside arrays [15].

Earth or nadir-pointing antennas provide coverage over the field of view subtended by the earth [18]. This footprint is achieved by optimizing both antenna directional beamwidth and orbit altitude. Geosynchronous [19] , telecommunication [20], and remote sensing [21] satellites utilize nadir-pointing antennas in

order to service the earth. Horn and planar array antennas are some types used for earth coverage [15].

Narrow coverage antennas are used to transmit very focused beams that require high gain performance. These requirements are imposed by either large data volumes (eg. payload data) or vast propagation distances (eg. deep space), and mainly use reflector antennas [18]. Reflector or dish antennas operate on geometric optical physics and have many design variations. Reflector antennas are usually large and intricate structures, and deployable membrane mechanisms have been developed to conserve space [22].

2.2 Phased Arrays

Antenna arrays are created by arranging multiple antenna elements in specific geometries and producing a larger aperture. The resulting field vectors interfere constructively where desired and destructively elsewhere, generating a more directive and higher gain radiation pattern. According to Balanis [15], there are five parameters that shape the overall pattern of the antenna:

- Geometrical configuration of the array (linear, circular, rectangular, spherical)
- Spacing in between elements
- Excitation amplitude of the individual elements
- Excitation phase of the individual elements
- Relative pattern of the individual elements

The spacing of the elements help reduce mutual coupling that cause parasitic losses. Varying the excitation amplitudes shape the field of view of the antenna. By applying a phase differential to each excitation, or "phasing", the beam can be electrically steered. Beam steering can be useful in cases where satellite pointing or mechanical actuation proves insufficient.

2.3 Microstrip Patch Antennas

The microstrip antenna configuration enables conformal printing on dielectric substrates using photolithographic techniques [10]. To this extent, feed networks, arrays, and other circuitry can also be implemented co-planar with the radiating elements. The open-ended nature of microstrip design allows diverse variations of antenna and feed geometries to be exploited. Many novel design techniques aim to enhance radiation performance or address shortcomings [25–35].

The mechanism of radiation is the excitation of a smaller metallic patch with reference to a larger ground plane, separated by dielectric material. The mismatch in size allows for the fringing fields at the edges of the patch to essentially radiate (see Figure 2.1(a)). On this note, the induced surface current density in a patch antenna exists in the plane of the conductors and the electric field in the dielectric is oriented perpendicular to this plane. This also produces a broadside radiation pattern shown in Figure 2.1(b).

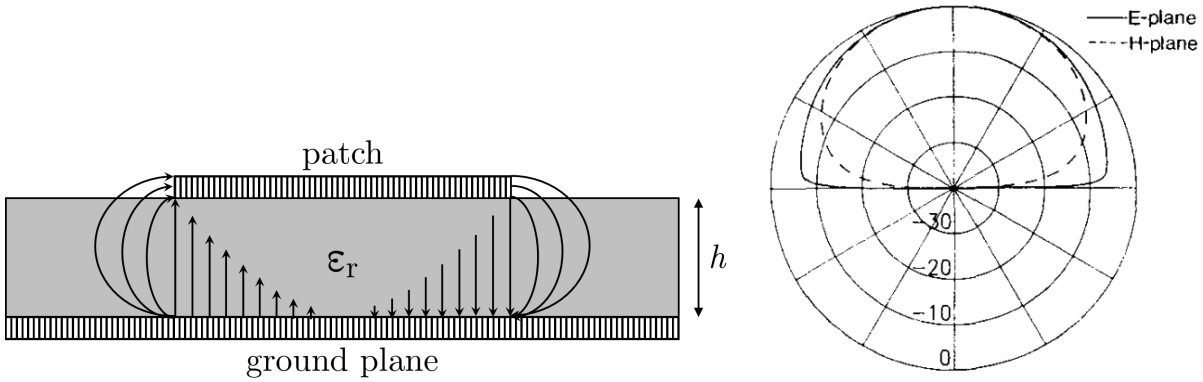

(a) (b)

Figure 2.1: (a) The radiation mechanism of a patch antenna by means of fringing electrical fields (side view), and (b) the radiation pattern of a simple patch antenna [10].

Microstrip patch antennas have been adapted for a wide range of uses, such as mobile communications, GPS, RFID, radar, even military and medical purposes [23,24]. Due to being driven by cost-effectiveness and miniaturization, CubeSats have given special attention to microstrip antennas. Tubbal et al. [16] evaluates the capabilities of various patch antenna designs using criteria for small satellite applications. There are many design techniques and approaches that can be employed to address the narrow bandwidth, lower gain, planar size, and non-steerable disadvantages of patch antennas. Bandwidth can be expanded by using con-

figurable polarization [25,26], different geometries for dual-band operation [27,28], and better feed matching techniques [29]. Gain improvement can be achieved by implementing arrays, which can also realize beam steering through sequential phase rotation [30,31] and differential phasing of the elements through power dividers [32]. Further miniaturization of the patch size can also be done through inverted F-configurations [28], meandering [33], shorting pins [34], and use of negative permeability metamaterials [35].

There are also many examples of patch antennas designed specifically for and implemented on CubeSat missions. Magalhaes et al. [36] analyzed an array configuration of four UHF patch antennas, but has increased risks from depending on four separate deployable mechanisms. Islam et al. [37] designed a single patch antenna with asymmetrical V-shaped slits on all corners to produce circular polarization (CP) and a parasitic strip for wide axial ratio (AR) beamwidth. This device has to be accommodated and mounted on the outside surface, complicating the integration process. Nascetti et al. [30] and Pittella et al. [38] both created CP antennas with sequential phase rotation by placing four elements orthogonally while phasing their excitations. This configuration allowed for the antenna and a camera lens to fit within a 10x10 cm^2 side. Both antenna devices have wide openings in the middle to accomodate cameras, and do not provide structural support. Padilla et al. [39] designed a programmable slot array for multibeam, omnidirectional, or directive radiation, but take up all available surface area of their 250x250x250 mm^3 spacecraft. Osorio and Ramirez [31] demonstrate a 3x3 square patch array, each comprised of a 2x2 sequentially rotated sub-array to achieve circular polarization.

The microstrip antenna design proposed for this research is a rectangular patch operating in S-band frequency. While the techniques discussed in this section involve intricate design geometries, the rectangular patch uses a more simplistic approach. Applying a simplified design benefits the novel manufacturing process and component accessibility explored in this research.

2.4 Composite Manufacturing Techniques

Advanced composite materials have benefited the aerospace industry by replacing aluminum or metallic structures with lightweight materials whilst maintaining strength for structural support [6]. Although the use of composite materials is prevalent in the aircraft industry, only recently are they being adopted for space flight on a limited basis [7]. Composite materials are comprised of a binding matrix reinforced by inclusions of various forms. Namely, CFRP is made of high strength carbon fibres bound by an epoxy resin matrix. The carbon fibres in the matrix can either be short and randomized or continuous long fibres arranged either unidirectionally or quasi-isotropic. Unidirectional CFRP has low off-axis strength, and thus rarely used in structures. In order to provide structural integrity in all directions, it is common practice to have at least 10% of fibre layers oriented in the 45° and 90° directions [40].

Two common manufacturing techniques to create CFRP for aerospace applications are using prepreg plies or infusing fibres with resin [40,41]. In the first technique, prepreg plies are sheets that contain one layer of fibres in a uniform direction and are pre-impregnated with uncured epoxy. These sheets are then stacked on top of each other in different orientations and cured in an autoclave at high temperatures to create a solid laminate. In the second technique, multi-directional dry fibres are placed and stacked inside a mold which is then infused with liquid resin, and cured to solidify. Holloway [41] states that the electrical performance of composite laminates depends strongly on the fabrication methods.

On the other hand, hybrid composites take advantage of the structural properties of carbon fibre while incorporating other materials to create lightweight and multifunctional structures. Combining dissimilar materials poses a challenge to the manufacturing process to accommodate various thermal properties to avoid the delamination of some layers. Ahamed et al. [42] use a ply-interleaving technique to join carbon and glass fibre materials and create an RF-transparent window for potential MFS antenna applications. Their research employs co-cured joints with resin pockets in two geometric configurations to improve the structural performance of the hybrid composite. Emmanuel [17] developed a two-step lamination process to manufacture hybrid structural radiation-shielding for spacecraft. The process involves a low pressure

lamination step to cure the carbon fibre composite layer and then an additional high pressure lamination step to cure the polyethylene fibre composite layer and consolidate a hybrid composite panel.

The proposed concept of the MFS antenna structure will also require careful integration of multiple materials with different thermal and mechanical properties. Much like the above literature, the manufacturing process has to be developed in order to avoid degradation of structural qualities and delamination of material layers. Typical methods of SU-8 deposition are modified and adapted in order to accommodate temperature limits of the hybrid composite panel.

2.5 Spacecraft Miniaturization

Conventional large spacecraft may take up a timeline of over five years from proposal to design, and cost anywhere from USD 100 million to 2 billion [3,13,14]. They also weigh upwards of 1000 kg and a few meters in height [3]. Technological advances have benefited the effort to push satellites to smaller sizes, such as nano- and pico-satellites. A special class called CubeSats typically weigh from 1-10 kg and sizes are based on a unit "U" which corresponds to a 10x10x10 cm^3 cube. Typical spacecraft dimensions include 1U, 3U, 6U and 12U (see Figure 2.2). They can also be built on shorter timeframes as quick as six months [14].

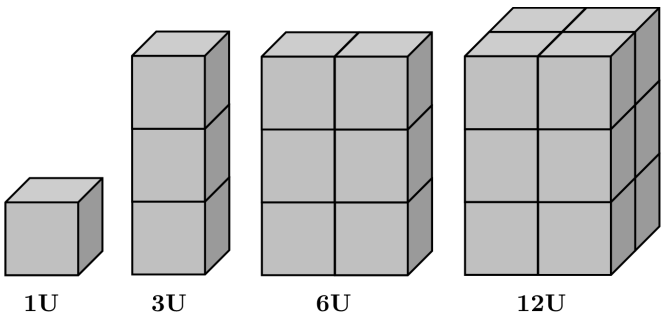

Figure 2.2: The most common CubeSat sizes are 1U, 3U, 6U, and 12U, where 1 "U" is a 10x10x10 cm^3 cube.

One of the main tenets of spacecraft miniaturization is to "do more with less". This design philosophy can be implemented by replacing one monolithic and expensive satellite with a constellation of smaller and cheaper satellites. This offers redundancy, and therefore, reliability in case of a single spacecraft failure.

The CubeSat platform is an example of miniaturized spacecraft that is notably popular with student groups and academic institutions, while progressively trending towards commercial uses [11]. By lowering the risks involved with loss or damage of property, they can be utilized as educational tools and even technology demonstration platforms. Overall, CubeSats cost less to build and the reduced size and weight enable for convenient ride sharing on rocket launches. Reference [11] shows the increase in CubeSat missions per year in Figure 2.3(a), and the percentage of those that are administered by universities and commercial companies. Figure 2.3(b) shows that a growing percentage of spacecraft launched per year are comprised of small satellites [12].

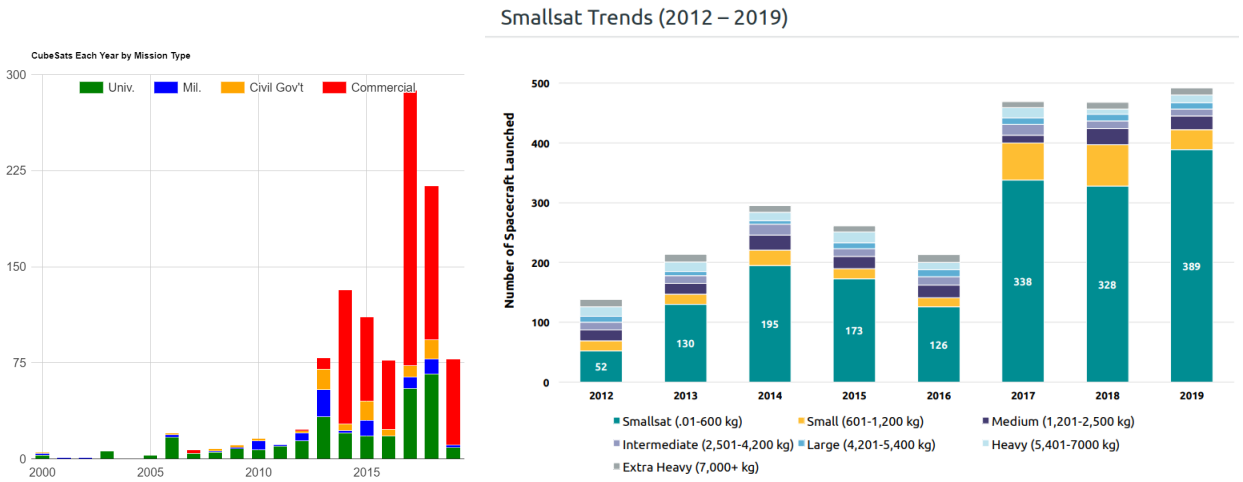

Figure 2.3: (a) CubeSat missions per year subdivided into university, military, civil government, and commercial uses [11] and (b) spacecraft launched per year subdivided into different size classes [12].

Standardized size constraints with constant increments set the stage for standalone, readily available, and adaptable components such as MFS. The development of a smart structural panel with increased functionality can be made available to CubeSat teams as a "ready to go" component that streamlines integration.

CubeSat programs open opportunities for groups to access space without the need for large resources, such as emerging and developing nations [43] and secondary schools [8]. Furthermore, CubeSats are a great educational tool for potential space system engineers in future missions as early as the middle school

level [81]. CubeSat opportunities help nations establish a previously non-existing space program and start space engineering education at an earlier stage.

CubeSats help expedite the qualification process of novel technologies that would be otherwise deemed as "too risky". To that end, more COTS solutions can obtain flight heritage which can then be adopted by future missions, adding reliability.

A couple of the more common antenna types used for small spacecraft are monopoles/dipoles for their simplicity, and reflectors for their high gain [13,14]. Although both types have their advantages, they are either protruding structures or have increased mechanical complexity as deployables. Protruding and cumbersome antenna structures violate size constraints and pose a higher risk of collisions and damage from MMOD. Deployable mechanisms take up valuable space, mass and power on the spacecraft, require more integration overhead, and adds the risk of deployment failure. Microstrip patch antennas, on the other hand, are an ideal solution to embedded smart panel technology due to their low profile and ease of fabrication [10]. They also display typically higher gains and directivity than monopoles and dipoles [15].

Tubbal et al. highlight in their survey [16] the various challenges and constraints imposed by small satellites on communications systems. These require the antenna design to have the following properties:

- Small size
- Lightweight
- Power efficient
- Robust communication capability

The size and weight restrictions can be addressed by the use of flat antennas and lightweight composites in MFS. There is also limited power available on-board, but patch antennas typically operate at lower power levels [23]. Efficiency is then improved through impedance matching by simple microstrip devices and power-saving by beam steering [16]. Finally, communication link durations and signal strength are improved

by increasing the gain with array configurations. Overall, spacecraft miniaturization offers an opportune platform to demonstrate the technological advantages of MFS.

2.6 Multifunctional Structures

The "do more with less" philosophy is also a significant driver for MFS technology development. Research by Guerrero et al. [45] estimates that MFS can reduce subsystem volume by 80%, mass by 90%, and assembly labour by up to 50%. MFS technology demonstrations can be dated as early as 1998 on NASA's Deep Space 1 (DS1) mission [46] and EO-1 mission in 2000 [47]. DS1 was a pioneering mission in developing MFS Technology Readiness Levels (TRL) as a technology demonstration. Structures are primarily designed to provide a rigid body that houses and supports the internal instruments of a spacecraft. It is common for these structures to also serve other purposes such as environmental shielding (radiation and debris) and thermal distribution, but are still fairly passive elements [48,49]. Modularized structure design [50,51] also demonstrates the ability for modules to function doubly as subsystem containers and the primary bus structure when stacked together.

It is inherent to spacecraft design that the mechanical structure subsystem has the most interfaces with all other subsystems (excluding flight software). This, along with its passivity, makes it the most versatile candidate for embedding additional functionalities. Aglietti et al. [48] and Sairajan et al. [49] review the state of the art in MFS and highlights the advantages and disadvantages of various examples.

Using novel technologies such as multichip modules and flexible circuit boards [46,47,52,53], electronics can be integrated into the structure, but increases the need for more cabling. These circuits can either be bonded onto a panel face or enclosed inside the structure [52], and used to control devices external to the satellite. Electronics can also be integrated into a sandwich panel with an aluminum honeycomb core. These methods have been demonstrated by embedding GPS receivers [52], sensors [53], actuators [54], energy storage [55], harnessing [52,56], communications electronics [57], and even entire electronic modules [58]. While beneficial, embedding these electronics can introduce difficulties to the integration process. Active devices

can be bulky and require accessible openings for harnessing and testing, whereas microstrip antennas consist of a passive thin conductive film. Embedding electronics into structures also complicates the thermal distribution and control, and leaves components prone to increased radiation doses that can affect critical circuit functionality.

On the other hand, antennas are already required to reside outside the satellite regardless of type, and are all designed to continue functioning in such environments. These characteristics make antennas a good candidate for embedded structural avionics that can be easily integrated.

Enhanced methods of thermal control can also be implemented through MFS. Embedding electronics within the structure makes it more difficult to conduct or radiate the generated heat away. Thermal control is required to maintain the embedded electronics within their acceptable operational temperature ranges. Jang et al. [52] performs a thermal analysis of MFS and the effects of added thermal paths within honeycomb cores. Rawal et al. [56] developed a radiator panel of composite materials with high thermal conductivity and validated by the DS1 mission [46].

Environmental shielding methods for spacecraft can also be reinforced by advanced designs that expand beyond the concept of just being a "wall". As the space around Earth is increasingly populated with various spacecraft, the risk posed by MMOD continues to grow. Cherniaev and Telichev [59] implement debris shielding achieved through "bumpers". According to [60], the ratio of radiation blocked to material thickness of CFRP is four times less effective than aluminum alloys. Emmanuel et al. [61] investigates the performance of different materials in various radiation environments. Most notably, Emmanuel's design of a polyethylene and carbon fiber hybrid composite proved efficient radiation shielding for highly elliptical satellite orbits [17,62]. Since radiation shielding is passively done by the structure, this enables us to improve and expand the uses of the MFS by introducing additional functionalities without compromising its structural integrity, such as microstrip patch antennas.

2.7 Multifunctional Structures with Antennas

One approach to multifunctional antenna structures is repurposing elements of pre-exisiting support structures. Sharawi et al. [63] embedded a 4-element printed monopole array with beam-forming capabilities in the wing struts of an unmanned aerial vehicle. By internalizing the antenna within already protruding structures (i.e. wings), drag is reduced, therefore reducing mechanical stress on the structure and communication subsystems. This design is custom-shaped to pre-existing struts, and are not as versatile for other uses. Matsuzaki et al. [64] investigate the use of rotor blades made with unidirectional CFRP laminates as antenna/sensors. The half-wavelength dipole is used as a sensor to detect rotor damage by observing any changes in the frequency response. Arenson [65] uses a cross-brace in the satellite frame to form a dipole. The device is made using additive manufacturing and is 10 cm long, the standard unit for CubeSats, but is not tested for structural support. Shirvante et al. [66] study the effect of deployable panels as reflectors for a radiating element. Gain performance shows improvement for monopole, extended parabolic reflector, and annular ring patch antennas for 1U and 3U CubeSats. Despite the improvements, dependence on deployable mechanisms increase the risk of failure.

A more advanced technique involves inserting the antenna elements within the structure. Baek et al. [67] design a conformal load-bearing array antenna structure (CLAAS) for state-of-the-art military aircraft. Radiating antenna tiles are supported by a multi-layer grid construction to create an array layout where shape can be customized by strategic placement of the tiles. This design leads to a more complicated manufacturing method and integration process, which this research is aiming to facilitate a solution for. Son et al. [68] create a smart-skin system by embedding microstrip antennas in a non-metallic honeycomb sandwich structure. The configuration is comprised of two parallel dielectric facesheets, each with patch antennas on the internal side, separated by a honeycomb core. The stacked patch design is used to increase bandwidth and the 4-bit digital phase shifter is used for electronic beam scanning. You et al. [69] created a similar construction as [68], but with an additional multilayer configuration, and using different materials for the dielectric, honeycomb, and composites for the external facesheets. Kim et al. [70] also used the same structural configuration but with a spiral-type microstrip antenna. Son, You, and Kim's approach to embedded antennas come closest

to my proposed design of a general-purpose load bearing panel. Their use of a honeycomb core structure adds a significant amount of volume to the component. Although these designs use commercially available dielectrics (such as RO4003 and duroid5880), my research seeks to investigate the use of atypical materials for the dielectric substrate.

There are also numerous studies characterizing the effect of embedded antennas on the load bearing abilities of the structure. Researchers have analyzed MFS characteristics such as the deformation and strain fields in [67], and impact [71], buckling [72], and fatigue [73] on the honeycomb sandwich structures. Santapuri and Bechtel [74] propose a mathematical model for the marriage of thermodynamics and Maxwell's equations in the field interactions and physical effects of hybrid mechanical-electrical systems.

Other researchers have looked into the interference effects of carbon fiber composites on electromagnetic radiation. De Assis and Bianchi [75] use a simplified composite model to asses the antenna figure of merit in the presence of CFC. Mehdipour et al. [76] test the radiation characteristics of a patch antenna operating against CFC and copper ground planes. Both studies show similar performance of CFC compared with aluminum or copper. Leininger et al. [77] demonstrate the variable grounding ability of CFRP, requiring metal conductors to divert fault currents and lower frequencies but featuring enhanced ground plane properties at higher frequencies. My research supplements these works by further investigating the effects of CFC on radiating electric fields.

Chapter 3

Materials and Characterization

3.1 Overview

This research endeavors to build upon the hybrid composite panel created by Emmanuel [17] from the University of Manitoba's Composite Materials and Structures Research Group (CMSRG) and create additional functionalities on top of radiation shielding. Emmanuel's hybrid uses advanced techniques to combine CFC and PFC materials, and adds a thin layer of aluminum to the outer faces of the panel (Figure 3.1). Through characterization, I investigate the extent to which each of the constitutive layers of this composite could be utilized as dielectric or radiative materials in the antenna system.

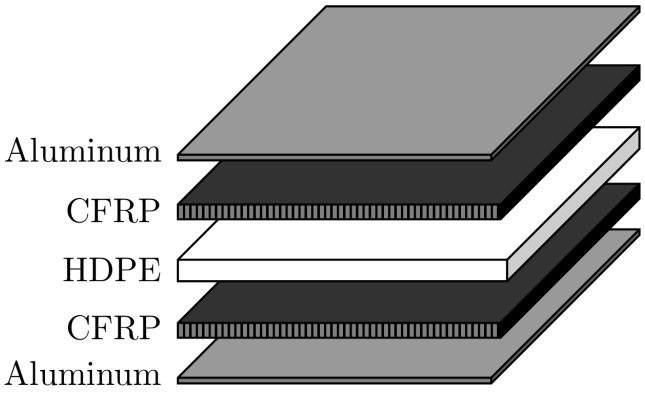

Figure 3.1: Stack-up showing the different material layers of the hybrid composite, with aluminum, carbon fibre reinforced polymer (CFRP) and high density polyethylene (HDPE) composites.

Material in this chapter has been published in the 70th International Astronautical Congress Conference Proceedings [81] and Acta Astronautica [82].

Materials need to be tested in order to determine their conductivity, permittivity, and loss tangent characteristics. Measuring conductivity determines whether a material layer is functioning as a conductor, which carries electric currents, or a dielectric substrate, which insulates and contains the electric field. The permittivity or dielectric constant is the capability of a material to store energy from an applied electric field, but more importantly, dictates the dimensions of the microstrip lines and antenna. The loss tangent measures how much of the radiation energy is dissipated within the substrate material, and is ideally minimized for power efficiency.

Hypothesis 2 (from Section 1.2) states that the CFRP can be used without detriment to antenna performance, which will be verified with simulations using data from characterization tests. In order to incorporate carbon fiber composites and their benefits into the MFS antenna, characterization determines whether CFRP can be utilized as a conductor or dielectric within the system. The tests discussed in the following sections will demonstrate the anisotropic nature of CFRP and shows both conductive and dielectric behaviour dependent on fibre orientation. This drove the choice to instead use an isotropic metallic conductor while still employing and benefiting from lightweight composites.

From the results, the aluminum face of the hybrid composite panel is designated as the ground plane structure of the antenna system, and an additional dielectric material layer is required. I propose the use of SU-8 epoxy as a candidate material for the antenna's dielectric substrate. SU-8 is typically used as a negative photoresist to develop high resolution microelectromechanical (MEMS) devices. This material was chosen due to its excellent adhesion to organic surfaces [78] and its adaptable methods for deposition.

In order to properly model and analyze these materials in RF design and simulations, all of the materials have to be characterized individually for their electrical properties. The following sections discuss the

experimental set-ups used and the respective material characterization results of CFC, PFC, and SU-8.

3.2 Test Equipment and Set-Up

The test equipment used for the following characterization tests include a vector network analyzer (VNA) from the University of Manitoba Antennas and Microwave Laboratory and a dielectric spectrometer from the University of Manitoba Advanced RF Systems Laboratory.

The first test set-up includes a copper microstrip line device on a dielectric substrate that is 6in x 6in in size. Measurement probes are placed on each of the two ends of the line and the S-parameters are measured. The Keysight N5224B VNA is used the measure the frequency response of the line from 500 MHz to 3 GHz. A diagram of this set-up is shown in Figure 3.2(a). This test is used twice to characterize and demonstrate both dielectric and conductive behaviour of the CFRP layers.

The second test set-up with the Solartron Analytical ModuLab XM uses a parallel plate configuration show in Figure 3.2(b). A sample is placed between two 40mm-diameter electrodes and the resulting complex impedance is measured, from which the electrical properties such as conductivity, permittivity, and loss tangent can be derived. Limitations of the dielectric spectrometer only allow us to measure up to 1 MHz which may result in a slight discrepancy between measured and theoretical values at 2.25 GHz.

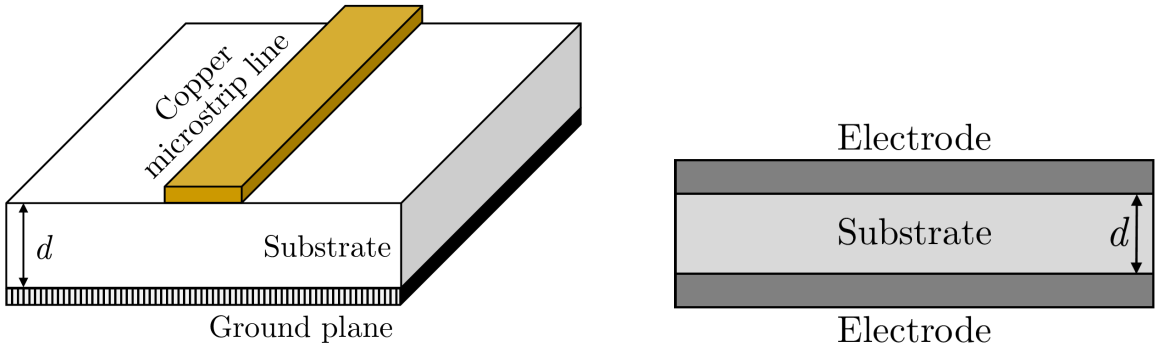

(a) (b)

Figure 3.2: (a) Microstrip line test set-up placing a dielectric substrate between a copper microstrip line and ground plane, measuring S-parameters between two ends of the line, and (b) dielectric spectrometer test set-up placing a substrate between two electrodes and measuring the impedance.

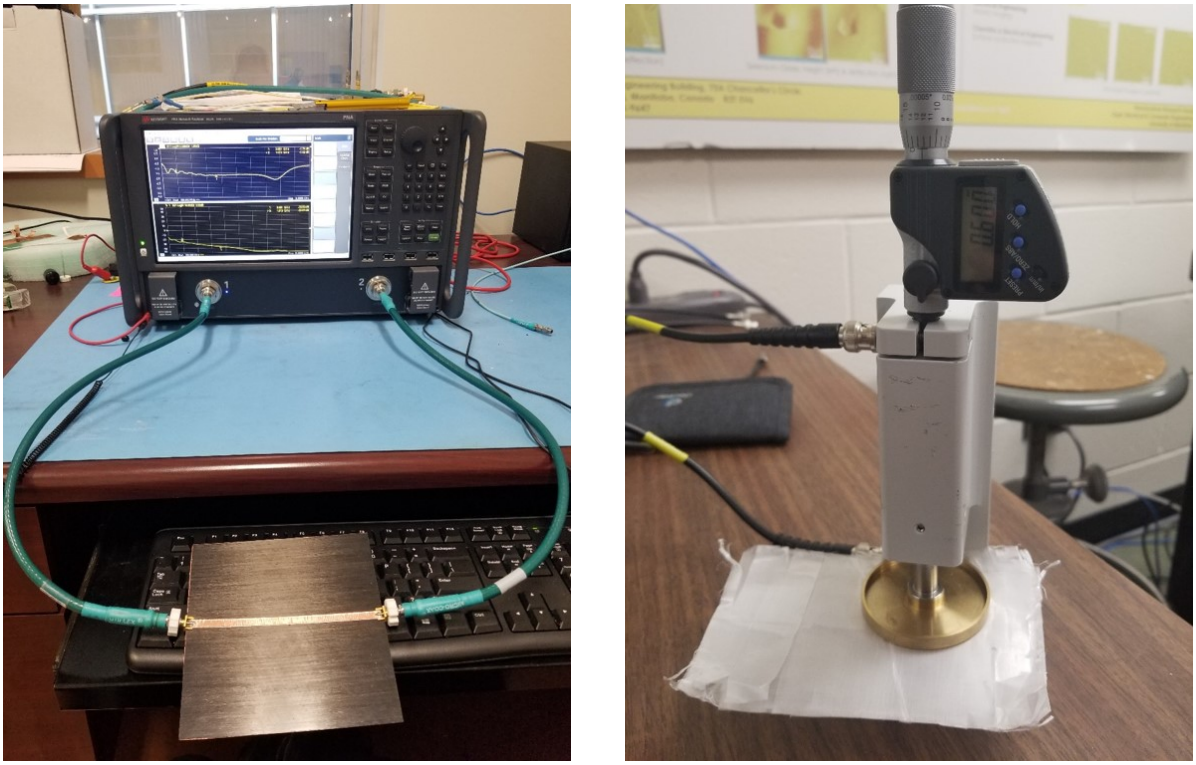

(a) (b)

Figure 3.3: (a)Test set-up for measuring a CFRP composite as a substrate using the dielectric spectrometer and (b) test set-up for measuring a HDPE composite using the dielectric spectrometer.

3.3 Carbon Fibre Composites

CFRP consists of conductive fibre rods in a non-conductive resin matrix, where the fibres are usually layered in 0°, 45°, -45°, and 90° directions. Seidel et al. [40] show that the anisotropic conductivity of CFRP laminates depends on the fibre orientation with respect to the incident electric field (E-field) using horn antennas, microstrip lines, and a patch antenna. The laminate acts like a conductor when the E-field is parallel to the fiber direction but acts like a lossy dielectric when the field is perpendicular. In the case of quasi-isotropic laminates where there is an even distribution of fibers in all directions, its performance depends on the orientation of the first or top-most layer. In my design, I utilize quasi-isotropic CFRP that has better structural performance than unidirectional laminates, which have poor strength in off-axis directions. In order to measure electrical properties in both orientations of the CFRP fibers, I used both test set-ups.

The first test assumes that the CFRP functions as a dielectric substrate and is placed between a copper microstrip line and a copper ground plane, as illustrated in Figure 3.2(a) and 3.3(a). In this set-up the microstrip line is oriented parallel to the top layer of carbon fibres. The S-parameters are measured and shown below in Figure 3.4. The plot does not display the typical notched frequency response that is characteristic for a microstrip device with a non-conducting dielectric (such as the shape in Figure 3.5). The reflection coefficient (S_{11}) is relatively high, within -5dB $< S_{11} <$ 0dB, and the transmission coefficient (S_{21}) is very low, down to a minimum of -60dB at higher frequencies. This shows that most of the current is immediately returned to the source ground, traversing down through the dielectric layer, instead of traveling through the length of the microstrip line towards the other probe. From these results, it can be concluded that the CFRP is conductive enough to be unsuitable as a dielectric substrate, since it does not provide enough electrical insulation between the microstrip device on the top and the ground plane on the bottom. This result was expected for the E-field in parallel case.

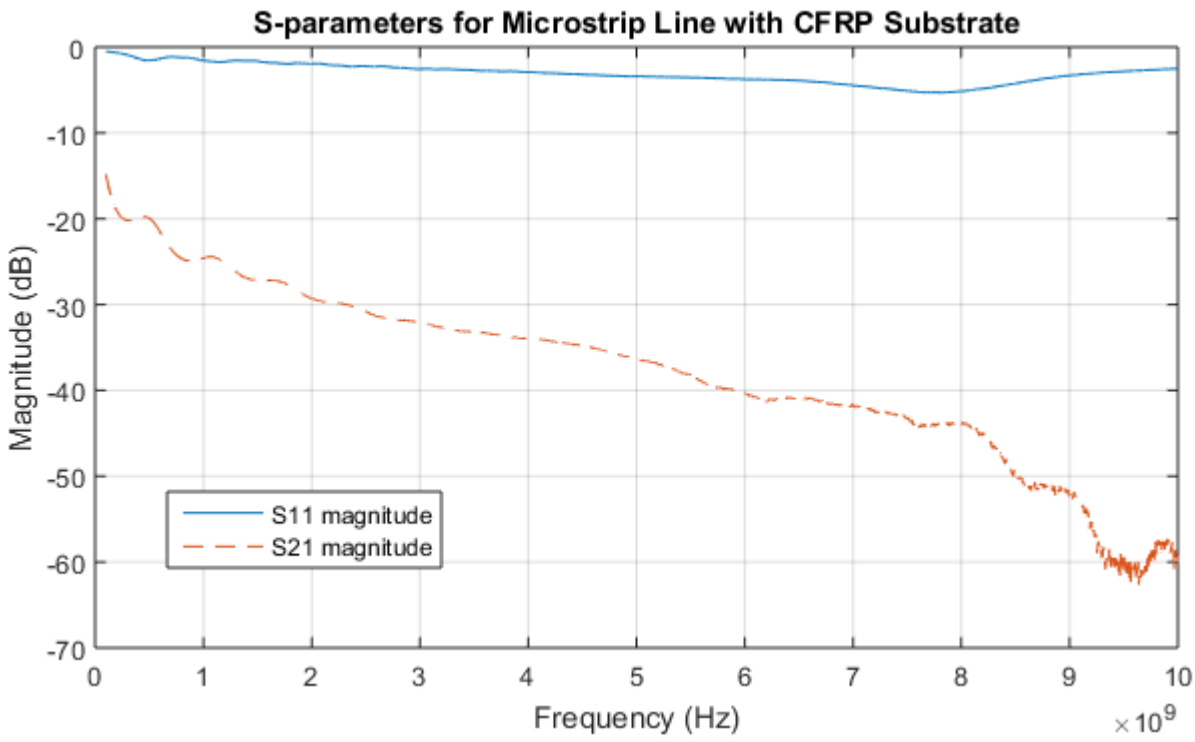

Figure 3.4: S-Parameters for a copper microstrip line on a CFRP dielectric substrate and a copper ground plane measured from 0-10 GHz.

The second test assumes that the CFRP functions as a ground plane and involves mounting a copper microstrip line on a foam substrate where $\varepsilon_{foam} \approx \varepsilon_{air}$ (Figure 3.2a). The microstrip line is again oriented parallel to the fibres in the first layer of the CFRP ground plane, and is expected to act as a good conductor. The resulting S-parameters are measured from 500 MHz to 3 GHz and shown in Figure 3.5. As expected, the microstrip device behaved normally as with a conductive ground plane, showing the opposite behaviour from the measurements in figure 3.4. The transmission coefficient is within -3dB $< S_{21} <$ 0dB, with minimal loss, in agreement with Seidel's results [40]. The S_{11} plot in figure 3.5 also shows minimal reflection losses at the harmonic resonances. Therefore, it can concluded that it is a good conductor at this configuration.

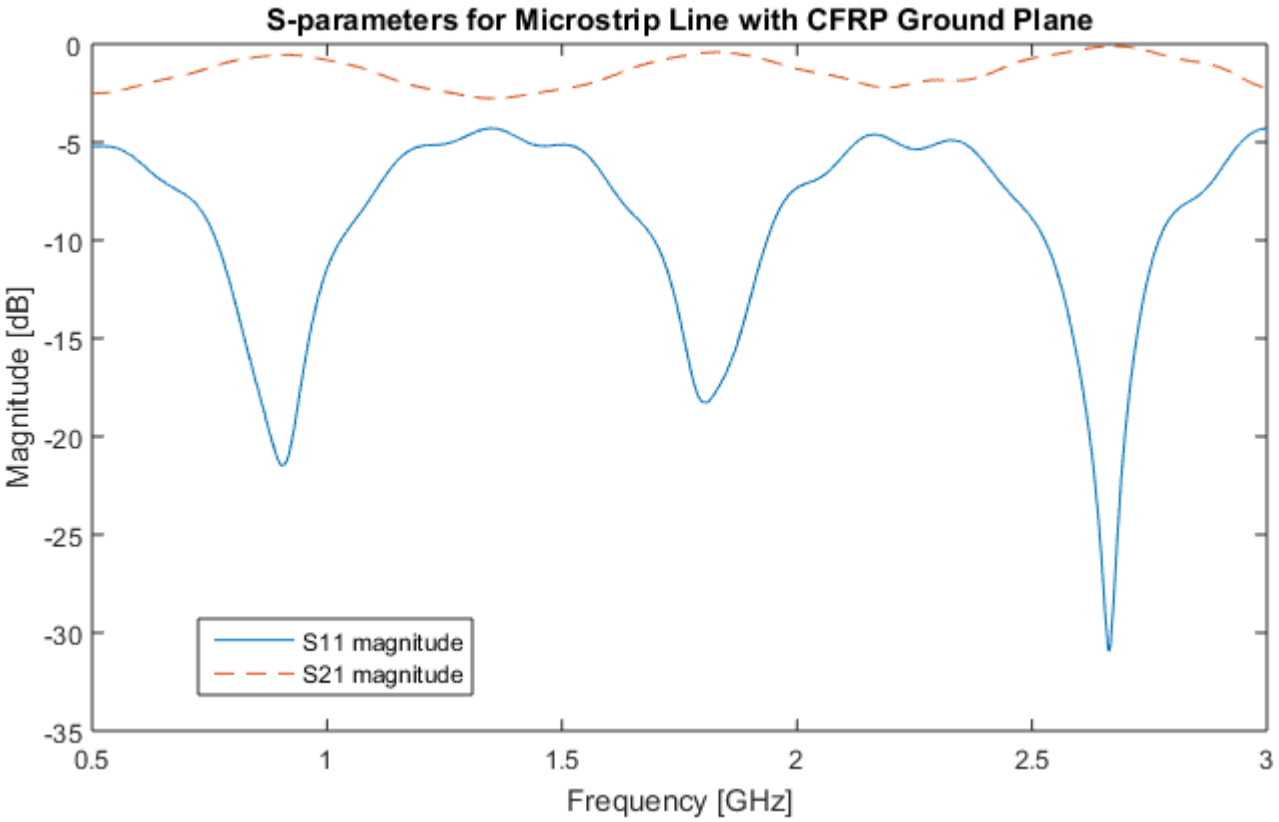

Figure 3.5: S-Parameters for a microstrip line parallel to the top layer of the CFRP ground plane fibres and a foam substrate measured from 0.5-3 GHz.

The third test involves analyzing the CFRP sample in a dielectric spectrometer, where it is placed between 40mm electrodes to create a parallel plate capacitor. In this configuration, the E-field of the capacitor is out-of-plane perpendicular to the multi-directional fibres. I can extract the electrical properties of the CFRP using the complex impedance at the frequency of 1 MHz shown in table 3.1. I can calculate the loss tangent ($\tan\delta$) and conductivity (σ) using equations (3.1)-(3.4), where f is the frequency, d is the thickness of the dielectric, A is the area of the electrodes, $Z^{'}$ is the resistance, $Z^{''}$ is the reactance, ε_0 is the permittivity of free space, and $\varepsilon_r^{''}$ is the imaginary part of the relative complex permittivity. The resulting low conductivity and non-zero impedance show that the CFRP acts like a lossy dielectric when the E-field is perpendicular, as expected.

$$\varepsilon_r^{'} = \frac{d}{2\pi f A \varepsilon_0}\left(\frac{Z^{''}}{Z^{'2} + Z^{''2}}\right) \tag{3.1}$$

$$\varepsilon_r^{''} = \frac{d}{2\pi f A \varepsilon_0}\left(\frac{Z^{'}}{Z'^2 + Z''^2}\right) \tag{3.2}$$

$$\tan\delta = \frac{\varepsilon_r^{''}}{\varepsilon_r^{'}} \tag{3.3}$$

$$\sigma = 2\pi f \varepsilon_0 \varepsilon_r^{''} \tag{3.4}$$

Table 3.1: Electrical properties of CFRP from dielectric spectrometer, perpendicular to E-field, measured and calculated at the frequency of 1 MHz.

Parameter	Measured Value	Calculated Value	Unit
Impedance $(Z^{'} + jZ^{''})$	38.5 - j198.7	-	Ω
Permittivity $(\varepsilon_r^{'} - j\varepsilon_r^{''})$	-	28.23 - j5.47	-
Loss tangent $(\tan\delta)$	-	0.1937	-
Conductivity (σ)	-	3.04 $\times 10^{-4}$	S/m

Both electrical performance tests of the CFRP show anisotropic conductivity in one case and lossy behaviour in another. Therefore this material is unsuitable for use as a conductive ground plane or a dielectric. From these results the aluminum layer will be used to function as the ground plane, while the inner layers of CFC and PFC maintain the characteristic light weight and durability of composites. Since the E-field in a patch antenna is out-of-plane perpendicular or normal to the ground plane (fig 2.1(a)), material properties from table 3.1 are used to model the CFRP in the next chapter.

3.4 Polyethylene Fibre Composites

There exists a thin layer of HDPE within the hybrid composite panel chosen for this research [17]. A sample of this composite with HDPE fibers in a polymer matrix was obtained from the Advanced Composite Materials Lab and measured similarly on the dielectric spectrometer. The sample is placed between two parallel plates as shown in figure 3.2(b) and 3.3(b). This material is non-conductive, acts like an insulating layer, and the extracted electrical properties using equations (3.1)-(3.4) at 1 MHz are shown in Table 3.2.

Table 3.2: Electrical properties of HDPE composite from dielectric spectrometer, measured at 1 MHz.

Parameter	Measured Value	Calculated Value	Unit
Impedance $(Z^{'} + jZ^{''})$	1.70 - j7482	-	Ω
Permittivity $(\varepsilon_r^{'} - j\varepsilon_r^{''})$	-	1.15 – j0.00026	-
Loss tangent $(\tan\delta)$	-	0.000227	-
Conductivity (σ)	-	1.45 $\times 10^{-8}$	S/m

Although the HDPE composite also has fibres oriented in different directions in a matrix, both components are non-conducting, and therefore does not have the same anisotropic behaviour as previously seen in CFRP. Due to the fact that this non-conducting layer is located in the middle of the hybrid composite stack-up, it electrically insulates the two opposite aluminum faces. This poses a manufacturing challenge since it restricts the ground connection to the aluminum face that the antenna is placed on, and eliminates the option of grounding on the bottom (opposite) face. This grounding issue is addressed later in Chapter 5 which explores the manufacturing methods I use.

3.5 SU-8

Due to the characterization results of CFRP, the hybrid composite panel's aluminum face has been designated as the ground plane, and a dielectric substrate material is still needed. SU-8 is an epoxy-based polymer that was chosen as a candidate dielectric for its low loss and excellent adhesion to inorganic surfaces [78]. This characteristic will help verify hypothesis 1 by depositing the antenna system on to the composite panel successfully without the need for adhesives or fasteners. It is typically used as a negative photoresist and patterned using UV for high-resolution MEMS devices [79]. In addition, SU-8 has low optical absorption to UV light after curing and high resistance to harsh chemicals. Once SU-8 is fully cured, the highly cross-linked structure provides high stability to radiation damage and low levels of outgassing in a vacuum. Melai [80] uses gas-chromatography and mass spectrometry to characterize the SU-8 volume outgassing to be 19 $\mathrm{l}\mu g\, cm^{-3}\, min^{-1}$, and at a level "comparable to Kapton" (which is commonly used on space vehicles).

Ghalichechian and Sertel [78] propose equations (3.5)-(3.6) for calculating the complex of permittivity of SU-8 at high frequencies based off previous models and experimental results, where the variable f is the frequency in terahertz. The second-order frequency-dependent equations are used with coefficients from Table 3.3 derived from testing partially and fully cross-linked SU-8 in order to solve for the complex permittivity. Curing the SU-8, or cross-linking, is the process of binding the polymer chains together for a solidified and stable structure. Using equations (3.5)-(3.6) with the fully cross-linked coefficients and at frequency $f = 2.25$ GHz, I calculate the theoretical permittivity, loss tangent, and conductivity listed in table 3.4. Fully cross-linked properties are considered in this antenna dielectric for a more stable substrate.

$$\varepsilon_r^{'}(f) = \alpha_1 + \alpha_2 f^2 \tag{3.5}$$

$$\varepsilon_r^{''}(f) = \alpha_3 + \alpha_4 f + \alpha_5 f^2 \tag{3.6}$$

Table 3.3: Coefficients for equations (3.5)-(3.6) for partially and fully cross-linked SU-8 [78].

Variable	Partially Cross-Linked	Fully Cross-Linked
α_1	2.95	3.25
α_2	-0.22	-0.33
α_3	-0.09	-0.05
α_4	-0.24	-0.20
α_5	0.13	0.09

I deposited a 1mm-thick sample of SU-8 on an aluminum plane, and measured it using the dielectric spectrometer set-up. Using measurements of the impedance from the spectrometer and equations (3.1)-(3.4), the permittivity, loss tangent, and conductivity are obtained and listed in table 3.4. It can be seen that the measured real permittivity is higher, the imaginary permittivity is lower, and the loss tangent is lower than the theoretical calculations. This discrepancy can be attributed to the difference in operational frequency of the measurements (1 MHz vs 2.25 GHz), which is a limitation of the dielectric spectrometer. Ghalichechian's paper [78] shows that as frequency increases, real permittivity decreases, imaginary permittivity increases,

and loss tangent increases.

Table 3.4: Electrical properties of SU-8 from theoretical calculations at 2.25 GHz [78] and the dielectric spectrometer measured at 1 MHz.

Parameter	Theoretical Value	Measured Value	Calculated Value	Unit
Impedance ($Z^{'} + jZ^{''}$)	-	29.69 - j4035.7	-	Ω
Permittivity ($\varepsilon_r^{'} - j\varepsilon_r^{''}$)	3.25 – j0.0504	-	3.54 – j0.0261	-
Loss tangent ($\tan\delta$)	0.0155	-	0.007357	-
Conductivity (σ)	1.45×10^{-6}	-	1.45×10^{-6}	S/m

These properties of SU-8 make it a viable candidate to be the dielectric substrate of the antenna. Although the loss tangent is higher than more well-known dielectrics (0.0027 for RO4003 [68] and 0.0009 for duroid5880 [69]), the deposition process of this material is an advantage as it can be shaped and adheres well. The relative permittivity of SU-8 also allows an S-band antenna design with dimensions that fit the CubeSat standard, discussed further in the next chapter.

3.6 Conclusions

Based on the characterization experiments, the proposed microstrip antenna will be constructed on top of Emmanuel's hybrid composite, with an SU-8 dielectric substrate and copper microstrip patch antenna shown in Figure 3.6. The hybrid composite panel's aluminum face has been designated as the antenna's ground plane.

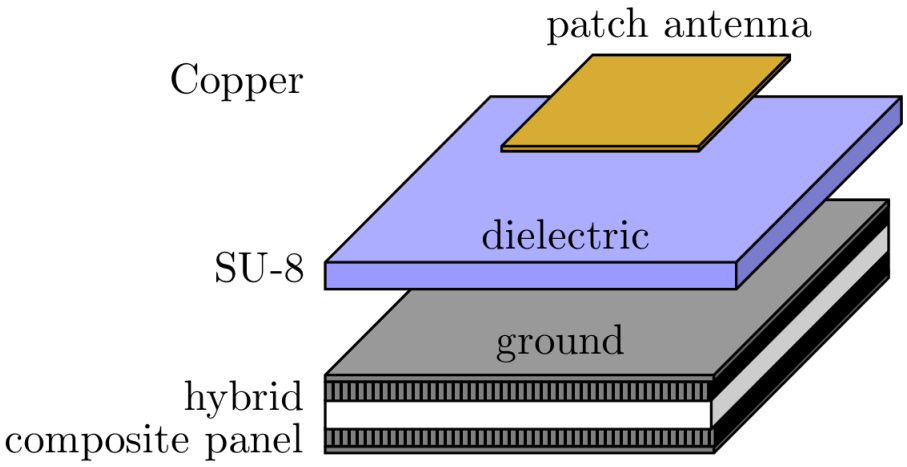

Figure 3.6: Stack-up showing the different material layers of the MFS antenna, with copper microstrip patch, SU-8 substrate, and a hybrid composite ground plane made of Al/CFRP/HDPE/CFRP/Al.

Although the discovery of CFRP's anisotropic behaviour seems to disprove hypothesis 2, the proposed design provides a solution to the issue. By utilizing a hybrid composite with an aluminum face, the ground plane structure can still benefit from qualities of CFRP without detriment to antenna performance. In addition, SU-8 partially verifies hypothesis 1 as a dielectric substrate with deposition properties that allow for adhesion to the ground plane structure.

The extracted electrical properties for all the materials will be used in the following chapter to model the entire antenna structure for high frequency performance. Although the primary antenna system includes the copper, SU-8, and aluminum layers, the presence of the other materials should be represented to properly analyze any radiation and parasitic behaviours of the entire MFS.

Chapter 4

Antenna Design and Simulations

4.1 Overview

The results from the material characterization tests are used to design and simulate a microstrip patch antenna and optimize performance. Using the calculated dimensions of the antenna and the stack-up geometry, a single element is simulated, expanded to a multiple-element array, and evaluated for phase-steering capabilities. The antenna's radiation performance is evaluated through extracted properties such as peak gain, bandwidth and beamwidth. Gain is a measure of the efficiency of the antenna along with its directional capabilities [15]. Bandwidth, for the purpose of this thesis, is defined as the frequency range in which the antenna reflection coefficient (S11) lies below -10 dB. Beamwidth, or specifically, half-power beamwidth (HPBW), is defined by IEEE as: "the angle between the two directions in which the radiation intensity is one-half the value of the maximum" [15] or 3 dB lower than the peak gain.

The extracted properties of the simulated antenna systems are used to evaluate their feasibility and potential applications for different spacecraft missions. The case studies investigated in this chapter include earth observation satellites, nanosatellites, and satellite constellations.

Material in this chapter has been published in the 70th International Astronautical Congress Conference

Proceedings [81] and Acta Astronautica [82].

4.2 Design and Model

The microstrip equations (4.1)-(4.4) from Balanis [15] are used in calculating the dimensions of the rectangular patch antenna. Where ε_{eff} is the effective permittivity, h is the height of the substrate, W is the width of the patch, ΔL is the length of the fringing fields, and L us the length of the patch. I use the dielectric constant for SU-8 calculated to be $\varepsilon_r = 3.25$ from Table 3.4, a substrate height of $h = 1$mm at a frequency of $f_r = 2.25$ GHz. The resulting patch dimensions are $W = 45.73$mm and $L = 36.98$mm.

$$\varepsilon_{eff} = \frac{\varepsilon_r + 1}{2} + \frac{\varepsilon_r - 1}{2}\left[1 + 12\frac{h}{W}\right]^{-1/2} \tag{4.1}$$

$$W = \frac{c_0}{2f_r}\sqrt{\frac{2}{\varepsilon_r + 1}} \tag{4.2}$$

$$\Delta L = 0.412h\frac{(\varepsilon_{eff} + 0.3)(\frac{W}{h} + 0.264)}{(\varepsilon_{eff} - 0.258)(\frac{W}{h} + 0.8)} \tag{4.3}$$

$$L = \frac{c_0}{2f_r\sqrt{(\varepsilon_{eff})}} - 2\Delta L \tag{4.4}$$

The respective thicknesses of each layer in the stack-up configuration (fig. 3.6) are listed in table 4.1. These dimensions and the characteristics extracted from Chapter 3 are used to realize an antenna model in ANSYS HFSS.

Table 4.1: Thickness, relative permittivity, and conductivity of each of the material layers in the smart panel antenna.

Layer	Thickness (h)	Relative Permittivity (ε_r)	Conductivity (σ)
Aluminum	75 $\pm$ 5 μm	-	3.8×10^{7} siemens/m
HDPE	3.8 $\pm$ 0.1 mm	1.15	-
CFRP	400 $\pm$ 0.38 μm	28.23	3.04×10^{-4} siemens/m
SU-8	1 $\pm$ 0.2 mm	3.25	-
Copper	2 $\pm$ 1 μm	-	5.8×10^{7} siemens/m

4.3 Single Element

Simulating a single patch element shown in Figure 4.1 with a coaxial probe feed results in the S_{11}, or reflection coefficient, plot in Figure 4.2 and the realized gain plot in Figure 4.3, with the properties summarized in Table 4.2.

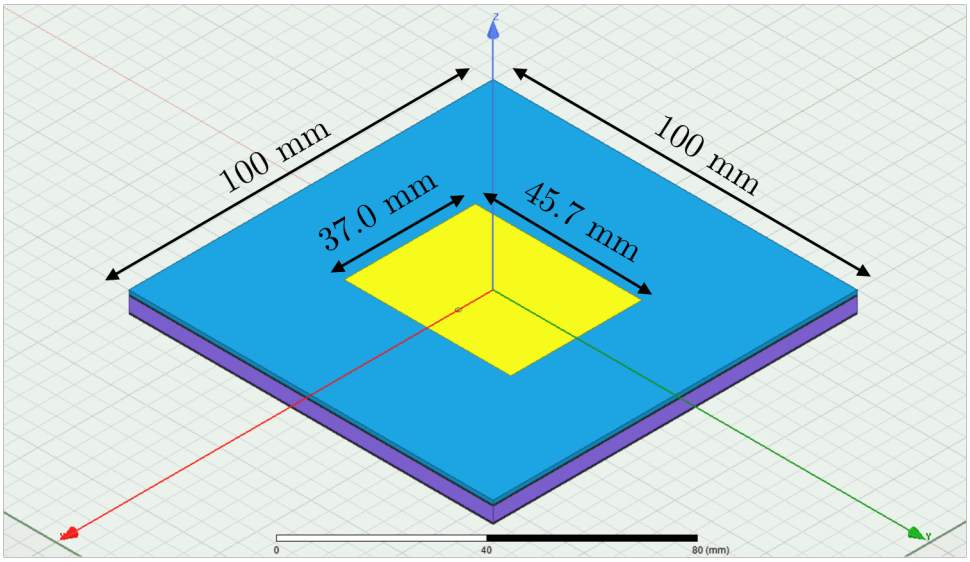

Figure 4.1: A single rectangular microstrip patch antenna on a SU-8 substrate and hybrid composite ground plane modelled in ANSYS HFSS.

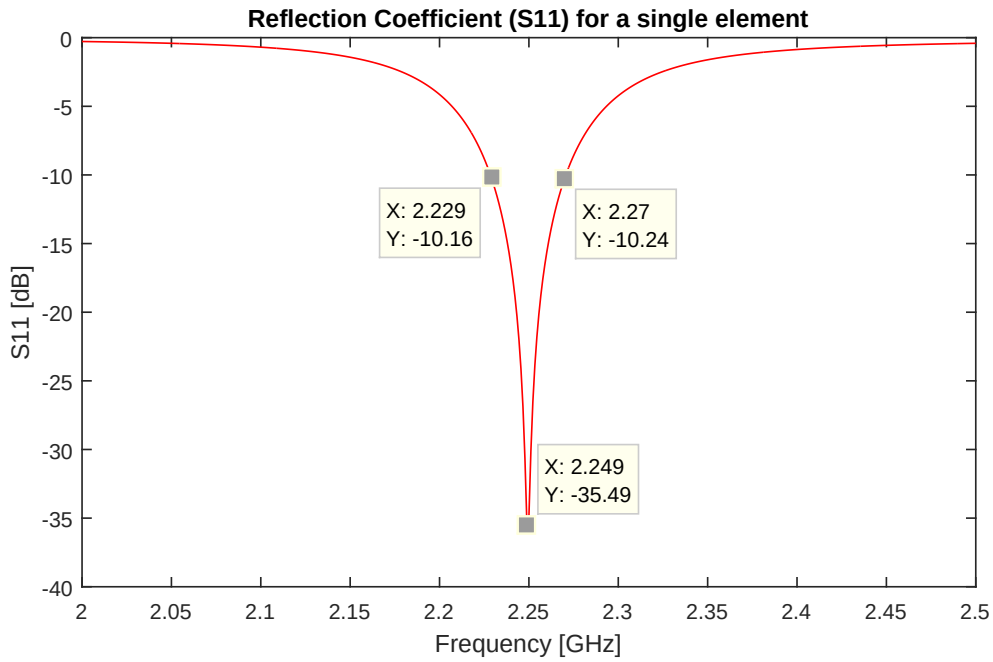

Figure 4.2: S_{11} reflection coefficient for a single antenna element showing the resonant frequency and bandwidth.

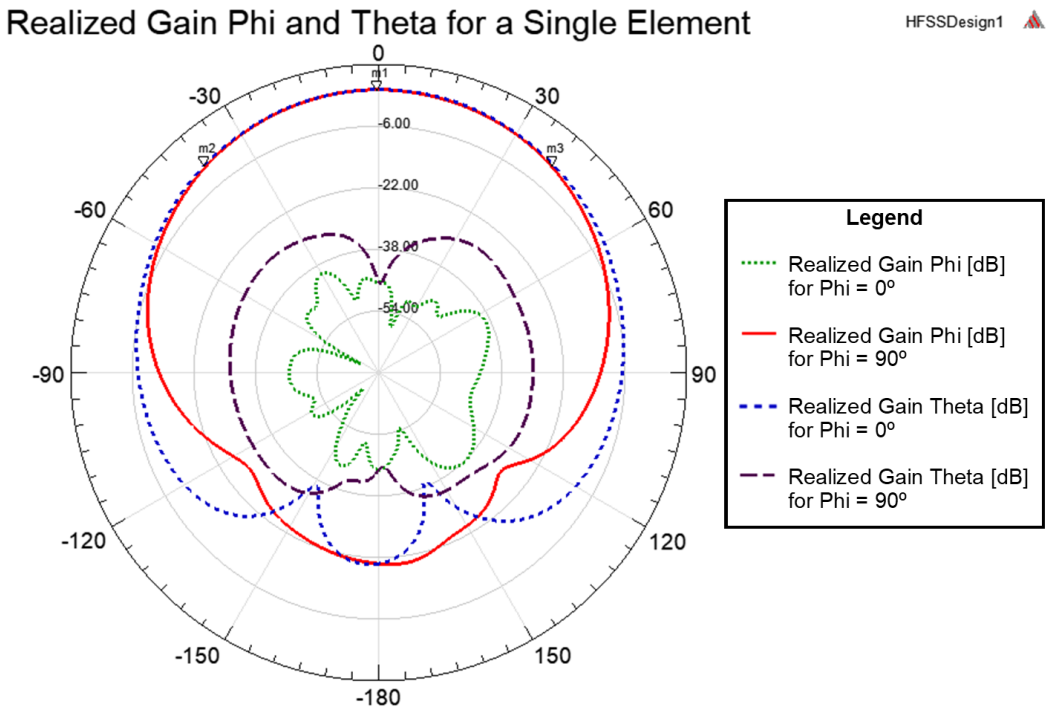

Figure 4.3: Realized gain plot for a single antenna element showing the half power beamwidth and peak boresight gain.

Table 4.2: Radiation properties of a single patch antenna element.

Parameter	Value	Unit
Center Frequency	2.25	GHz
10dB Bandwidth	40	MHz
Reflection Coefficient	-48.9	dB
Peak Gain	3.4	dB
Half-Power Beamwidth	80	degrees

The results from this section show expected radiation performance on the lower end of S-band patch antenna designs highlighted by Tubbal [16]. The lower gain levels can be attributed to the lack of specialized design techniques that are utilized in the examples from the reference. Although this is a disadvantage, the decision to use a simplified design is beneficial for streamlining a manufacturing process. In addition, the single element patch antenna gain outperforms that of dipole antennas [15], which is a popular choice for most CubeSat missions [13].

4.4 Planar Array

The initial design is expanded into a 3x3 rectangular array shown in Figure 4.4, with a half wavelength element spacing on the surface area of a 6U CubeSat (30cm x 20cm). The results show an enhancement of the gain from 3.4dB to 12.1dB and increased directivity with a smaller HPBW. A consequence of building an array creates grating lobes and added null points.

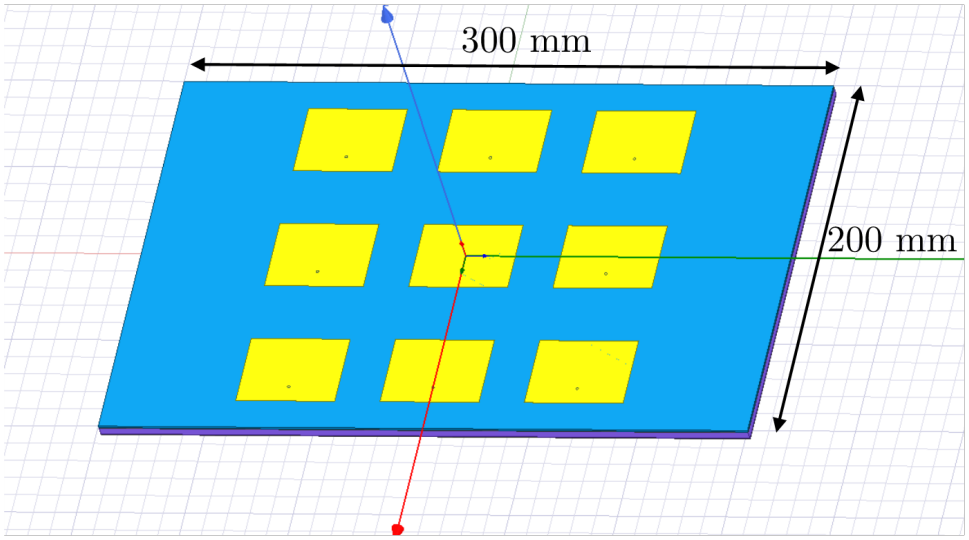

Figure 4.4: A 3x3 array of rectangular microstrip patch antennas on a SU-8 substrate and hybrid composite ground plane modeled in ANSYS HFSS.

The properties are summarized in Table 4.3, extracted from the realized gain plot in Figure 4.5. Figure 4.5 shows low cross-polarization effects of the antenna, <-27.5dB in theta and <-42.5dB in phi polarizations. Figure 4.6 shows mutual coupling effects between all the array elements (<-23dB), which represents the power radiated from one element and absorbed by the others. Figures 4.5-4.6 demonstrate minimal parasitic power loss within the antenna structure.

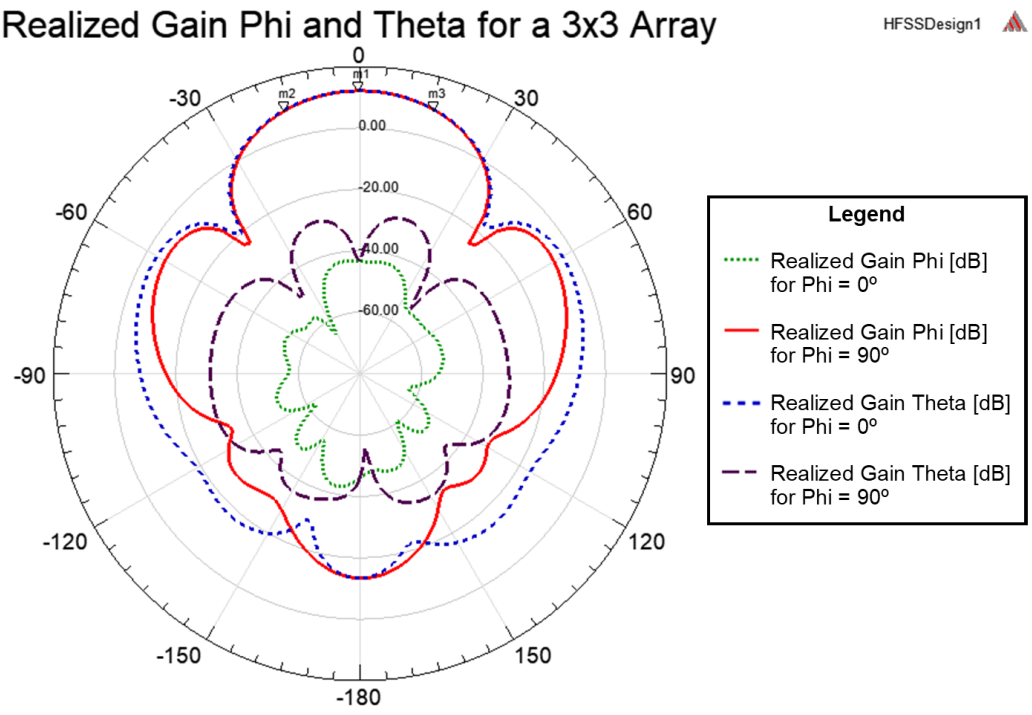

Figure 4.5: Realized gain plot for 3x3 antenna array showing the half power beamwidth and peak boresight gain.

Table 4.3: Radiation properties of a 3x3 antenna array.

Parameter	Value	Unit
Center Frequency	2.25	GHz
10dB Bandwidth	40	MHz
Peak Gain	12.1	dB
Half-Power Beamwidth	32	degrees

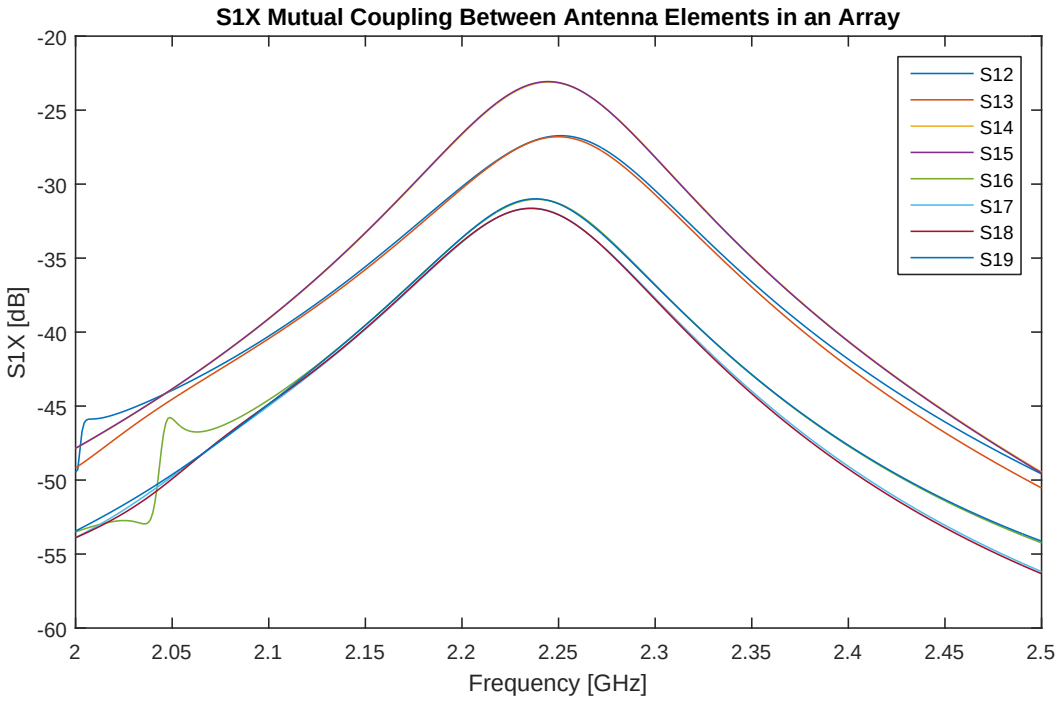

Figure 4.6: S_{1X} Transmission coefficient plots showing mutual coupling between all elements in the array.

It should be noted that Figure 4.6 displays the S_{1X} transmission coefficients between the middle element and all 8 surrounding patch elements, for x from 2 to 9. Noting that all the curves for these S-parameters fall below -20dB, it can be assumed that coupling is at negligible levels.

The results from this section show improved gain performance from the single element from 3.4 dB to 12.1 dB with the 9-element array and increased aperture size. This allows for high data rates and higher speed communications that require an antenna gain around 12 dB [14].

4.5 Phased Array

Applying a phase difference to the excitations of the individual patches allow for changing the direction of the beam. The beam can be scanned in the X and Y directions and the angle range and peak gain for each direction is shown in Figure 4.7 below. The beam can be scanned in the X-direction with a maximum scanning range of θ = [-50°, 50°] and a minimum peak gain of approximately 7.5 dB. Additionally, the beam

can also be scanned in the Y-direction with a maximum scanning range of θ = [-46°, 46°] and a minimum peak gain of approximately 6 dB.

The maximum angle with the minimum gain can be achieved by applying a 180^{o} excitation phase difference to each row or column of patch elements. It should be noted that with this phase difference, two symmetrical peaks are obtained at the outer angles simultaneously.

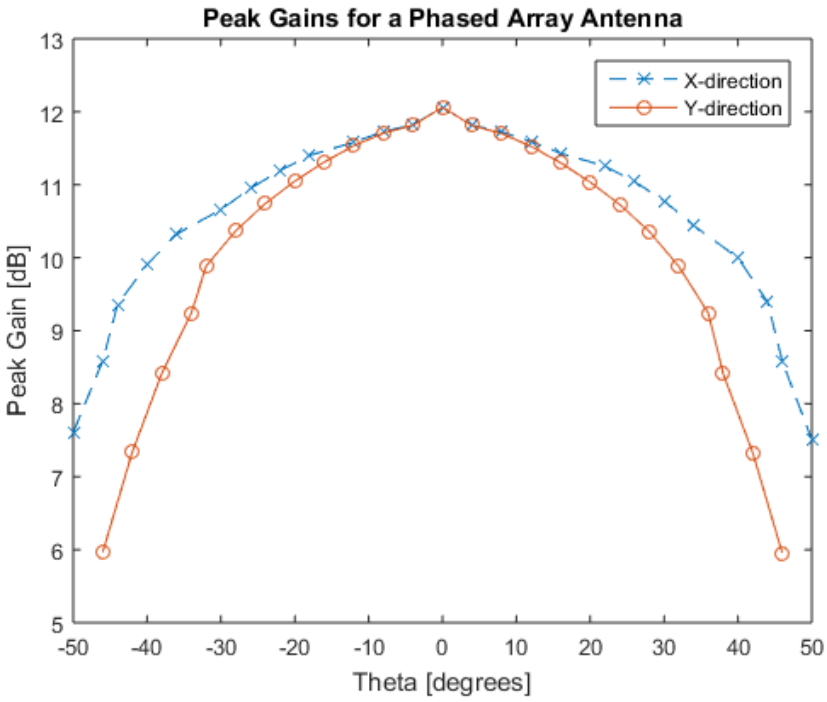

Figure 4.7: Peak boresight gains for each scanning angle in both X- and Y-directions.

By studying the radiation performance of a phased array system, I can determine the range capability that the antenna beam can be steered. Since the implementation of the array concentrated more power at the boresight and beamwidth was narrowed from 80° to 32°, this can limit the range of "sight" of the antenna. Phase steering can compensate for this loss and allow the antenna to direct its beam in other directions away from the surface normal angle (perpendicular). From the results, the total range of the antenna is increased to over 90°, while maintaining a peak gain of 6-12 dB, which is comparable to the antenna gains discussed in [16]. In addition, the implementation of electrically steered antennas help reduce risks from mechanical failure by removing moving parts on the spacecraft.

4.6 Case Studies

This section studies the concept of a MFS antenna for use in three distinct potential use cases (a large radar mapping spacecraft, CubeSats and a constellation of small spacecraft to provide a data backhaul service), illustrated in Figure 4.8. The following subsections describe each application.

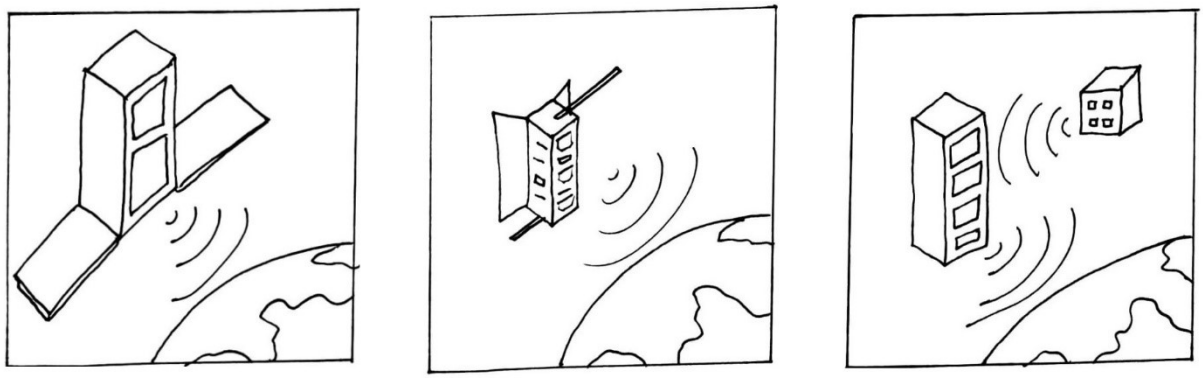

(a) (b) (c)

Figure 4.8: Potential use case studies using MFS antennas for (a) earth observation satellites, (b) CubeSats, and (3) satellite constellations.

4.6.1 Earth Observation Satellites

Earth observation satellites, especially radar mapping, have many practical applications such as agriculture, meteorology, and environmental sensing. An example is the RADARSAT Constellation Mission (RCM) which is a Canadian space mission that consists of a fleet of three satellites for earth observation using synthetic aperture radar (SAR) [83]. While the SAR system uses C-band frequencies for imaging, RCM uses S-band frequencies for tracking, telemetry and command (TT&C). The frequency band for this case falls within the allocated spectrum for earth exploration satellite space operation and space research down-link [84]. The RCM uses Thales Alenia's integrated S-Band transponder (ISBT) [85] to operate TT&C, which is evaluated for compatibility with the MFS antenna. Although the designed operational frequency of 2.25 GHz falls within the range of the ISBT's transmitter, it falls outside the tuning range of the receiver. This can be resolved by modifying the patch length to shift the operational frequency appropriately.

According to [14], high data rates with an acceptable signal to noise ratio require antenna gains of about 12 dB, which was achieved by the 3x3 planar array. Using the Nyquist bandwidth (equation 4.5), I estimate a simplified assumption for the maximum data rate (C) that can be achieved from a 40 MHz bandwidth to be 40 Mbps for binary (M=2) or 80 Mbps for quadrature (M=4) communications. In comparison to [85], where the receiver can operate with receiver bit rates up to 2 Mbps and transmitter bit rates up to 8 Mbps.

$$C = B \log_2 M \tag{4.5}$$

The RCM currently occupies a sun-synchronous orbit with an altitude of roughly 600 km [83]. The free space path loss (FSPL) equation is shown below in (4.6) where d is the distance or altitude, f is the operating frequency (2.25 GHz), c is the speed of light, and G is the antenna gain of the transmitter (tx) or receiver (rx) in dB. The receiver antenna gain can be set to 0 dB to find the signal power at ground level. Using this formula, the FSPL is calculated to be around 143.0 dB at an altitude of 600 km with a transmitter gain of 12 dB at 2.25 GHz. Noting the RF output power of up to 37 dBm from [85], the power level of the signal to earth at ground level will be roughly -106 dBm, which is a sufficient level for detectable signals. This result is comparable to the acquisition threshold of [85] which is -128 dBm.

$$FSPL = 20 \log_{10}(d) + 20 \log_{10}(f) + 20 \log_{10}\left(\frac{4\pi}{c}\right) - G_{tx} - G_{rx} \tag{4.6}$$

The RCM satellites are approximately 3.6 metres tall and represent traditionally larger sized spacecraft. This allows for larger antenna aperture sizes which increases the gain, and benefits missions such as earth observation satellites that generate high volumes of data. Considering the SAR antenna dimensions of the RCM to be 6.75m x 1.38m [83], the 12 dB array's size of 20cm x 30cm is significantly smaller and can be fitted onto the nadir-pointing surface easily. Expanding upon this in a larger array, an aperture area of 1m^2 can fit up to a 10 x 10 planar array and simulations yield an increased gain up to 25 dB. Finally, observation satellites that scan the surface of the earth can benefit greatly from the implementation of phase-steerable arrays.

4.6.2 CubeSats

CubeSat teams often operate their own ground stations for satellite TT&C which rely on amateur radio operators. Incorporation of amateur radio increases the accessibility of space missions to different users such as students and worldwide operators. The operational frequency band can be modified to fall within the allocated spectrum in the S-band for amateur use [84], and used for space-to-earth communications. The miniaturized dimensions of CubeSats as small as 1U imposes a strict restriction on available space and lends to smaller antenna apertures.

The single antenna element simulated earlier is located on a 10cm x 10cm composite panel to represent a single 1U face of a CubeSat. The single element gain of 3.4 dB is higher than the typical gain of dipoles around 2.15 dB [15], which is a commonly used type of antenna for CubeSats. Although dipole antennas are omnidirectional and have a wider range of sight than a patch antenna, this can be compensated by placing patch antennas around 4 faces of a CubeSat to create a pseudo-omnidirectional pattern as is the configuration in [36]. A drawback of this concept is the occupation of the already limited real estate on the surface of CubeSats. Another typical size used by CubeSats missions is 6U, which has dimensions of 10cm x 20cm x 30cm. This was assumed earlier in the simulation of a 3x3 planar array.

A reasonable power allotment for small satellite missions can be assumed to be around 1 Watt or 30 dBm. Another typical mission parameter for amateur CubeSats is to reside in low earth orbit, or approximately 400 km [86]. Using the free space path loss equation (4.6), with a single element gain of 3.4 dB, the power level of the signal to earth at ground would be -118.1 dB, which is detectable by ground station transceivers with less limitations on antenna sizes. A standard data rate of 9600bps is a popular design for most amateur satellites, such as [51], which is also achievable by the antenna bandwidth of 40 MHz, as calculated earlier with equation (4.5).

4.6.3 Nanosatellite Constellation

Satellites in a low-Earth orbit backhaul constellation create a communication relay network that can be accessible to operators of amateur satellites. Having a communication relay can help satellite operators by eliminating the need for independently-run ground stations. The opportunity to outsource and streamline ground station operations to dedicated constellations can benefit the increasing commercial use of small satellites.

In general, satellite constellations that are required to perform space-to-space communications will need a large range of sight, as opposed to nadir-pointing ground communications. The directive nature of patch antennas would not be ideal in these situations, unless configured to simulate pseudo-omnidirectionality. For this purpose, I assume an orbital plane of satellites in a constellation at low earth orbit (400km altitude). In order for a transmitted signal to traverse the intersatellite distance using antenna array (12dB gain) with sufficient power (>-128dBm), the distance should be no more than 3000km. This corresponds to an equivalent of at least 15 satellites in a single orbital plane.

Adding phase-steering capabilities to antennas in nanosatellite constellations can help overcome the disadvantages of using directive patch antennas. Overall, the use of patch antenna arrays for this application would not be deemed viable due to the directional requirements of intersatellite communications. While directive antennas prove advantageous for space-earth communications, intersatellite links require more omnidirectional patterns that would not occupy 4 out of 6 faces of a satellite. This is especially significant for small satellites with limited surface area.

4.7 Conclusions

This chapter illustrates a rectangular patch antenna design and its expansion into a multiple-element phased array system. Simulations performed in ANSYS HFSS provided results where performance parameters such as operational frequency, bandwidth, peak gain, beamwidth, and scanning range are extracted. Using these

properties, the application of the proposed MFS antenna design is analyzed for different case studies such as large satellites, small satellites, and satellite constellations.

The case studies showed that larger spacecraft such as earth observation satellites have enough surface area and available power to support large aperture patch antenna arrays. They also have high pointing accuracies due to the nature of their mission that allow directive antennas to be pointed accurately towards earth for space-earth TT&C communications. On the other hand, CubeSats that are inherently smaller and have less available power cannot support large arrays. A single patch antenna is still a viable option for use in CubeSats due to their higher gain performance and space-saving benefits, while directionality can be modified using different array geometries. Finally, due to the conflicting nature of intersatellite links and directive patch antennas, the design is not a practical choice for nanosatellite constellations, since they are limited in size and require a wide range of sight.

Through the simulation results and case studies, hypothesis 3 can be partially verified for large and small satellites operating space-earth communications, pending experimental results. The hypothesis states that the proposed MFS antenna design will meet the performance standards of satellite communications. In this case, the radiation performance is sufficient for directing radio signals in a specified direction (towards earth). Additionally, hypothesis 4 can also be verified with the dimensions of a single antenna panel which is 10cm x 10cm x 5.75mm or a 3x3 array with dimensions 20cm x 30cm x 5.75mm. The hypothesis states that the MFS antenna can reduce the component footprint and maximize useable spacecraft volume. The thin planar profile and ability to fit onto a 1U size for CubeSats show that the proposed design can be beneficial for space miniaturization efforts.

Chapter 5

Manufacturing Methods

5.1 Overview

The smart panel antenna structure is realized by the combination three components: a hybrid composite ground plane, an SU-8 substrate, and a copper microstrip patch antenna device. This chapter presents the methods and manufacturing procedures used to amalgamate all the components that forge an MFS antenna. The hybrid composite is manufactured by the University of Manitoba Composite Materials and Structures Research Group (CMSRG), while the SU-8 deposition and copper sputtering are done at the University of Manitoba Nanosystems Fabrication Laboratory (NFSL). Material in this chapter has been published in the 19th International Symposium on Antenna Technology and Applied Electromagnetics Conference Proceedings [87].

5.2 Hybrid Composite Panel

The hybrid composite panel was created by Emmanuel [17] and is comprised of three materials: polyethylene fibre composite, carbon fibre composite, and aluminum alloy. A carbon fabric pre-preg and a woven fabric of ultra-high molecular weight polyethylene (UHMWPE) impregnated with a low-density polyethylene (LDPE) film are used. Due to the difference in the viscosities of the LDPE versus epoxy matrices, Emmanuel developed a two-step lamination process using low and then high pressure subsequently. The first lamination

step uses low pressure to cure the CFC and bond all the layers together. The second step then uses high pressure to cure the PFC and consolidate the hybrid composite. This composite panel is the base of the MFS antenna and the following components are installed on top.

5.3 SU-8 Deposition

SU-8 2075 negative photoresist from MicroChem is used [88]. The deposition was done in multiple layers to achieve the desired substrate height, in this case, a 0.85 mm thick substrate. I modified the method of SU-8 deposition for other materials (*eg.* aluminum) previously developed by the NFSL to comply with temperature constraints of the hybrid composite panel. Initial baking trials have shown that the hybrid composite experiences delamination or debonding of the layers beyond 100°C and cooling rates higher than 4°C/sec. According to Thompson [7], spacecraft structures in orbit are expected to experience temperature extremes of -45°C to 60°C. The following steps dictate the SU-8 deposition method for the hybrid composite panel:

1. The composite panel is rinsed first with acetone, then isopropanol, then de-ionized water, and finally dried with N_2 gas.
2. A tape mask is applied at one of the edges to leave an exposed area of the aluminum foil for an electrical connection to the ground plane.
3. Liquid SU-8 is poured onto the panel as shown in Figure 5.1.*
4. The panel is vacuum gripped to a spinner in Figure 5.2 and spun at 600 rpm for 25 seconds, then at 1000 rpm for 30 seconds.
5. The SU-8 undergoes a soft bake on the hotplate in figure 5.3 at 65°C for 20 minutes, then at 95°C for 90 minutes.
6. Repeat steps 3-5 until the desired substrate thickness is acquired.
7. It is then exposed to ultraviolet (UV) light four times, for 20 seconds each, for a total of 80 seconds.**

8. A post-exposure bake on the hotplate in figure 5.3 at 65°C for 6 minutes and 95°C for 20 minutes.

9. A final hard-bake to cure and stabilize the SU-8 is done at 100°C for 60 minutes.†

* Pouring 1ml of resist for each inch (25mm) of substrate diameter is recommended by the datasheet. [88]

** Near UV 350-400 nm. Intermittent exposure duration as per manufacturer recommended process.

† For the final hard-bake, it is recommended that a curing temperature is 10°C higher than the maximum expected operating temperature.

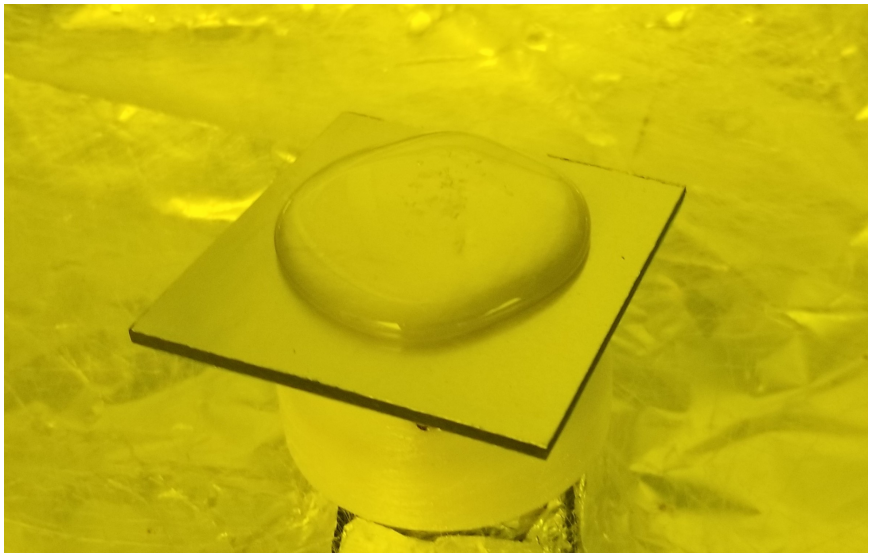

Figure 5.1: Liquid SU-8 is poured on top of the hybrid composite panel.

Figure 5.2: The machine used to spin SU-8 at 600 and 1000 rpm.

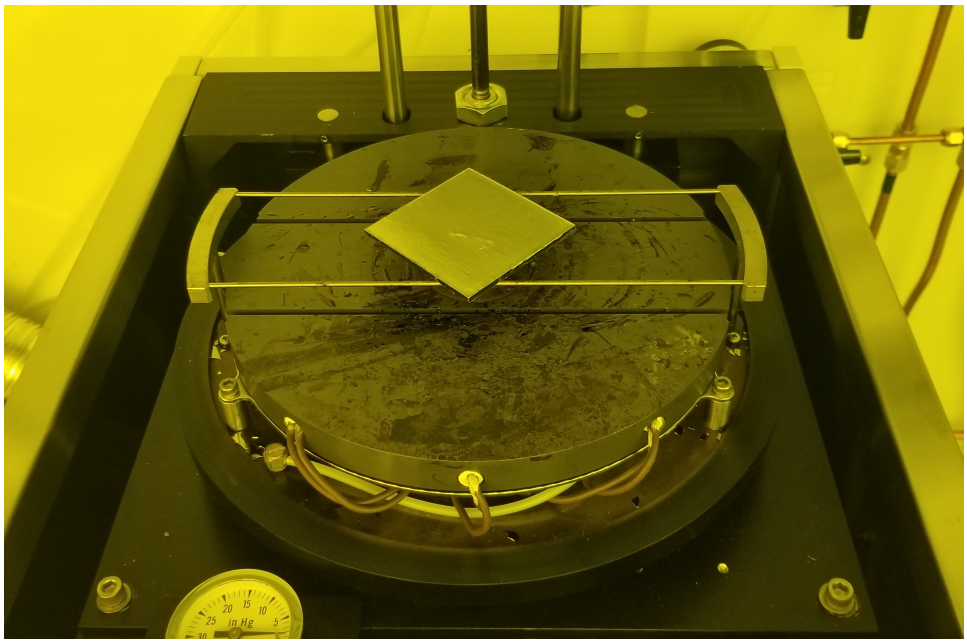

Figure 5.3: The hot plate used for soft-bake, post-exposure bake, and hard-bake of the SU-8 at various controlled temperatures.

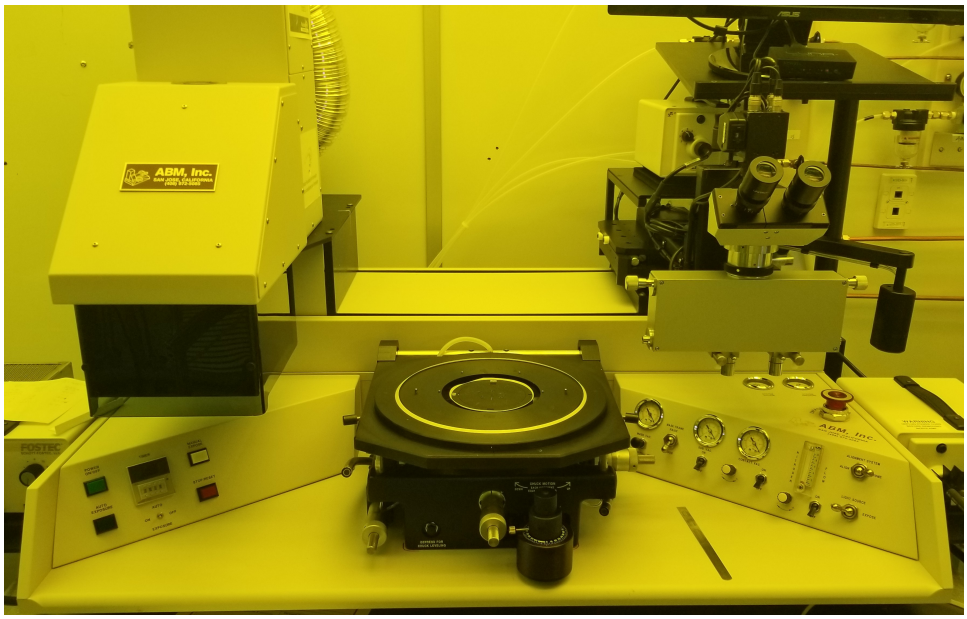

Figure 5.4: Ultraviolet (UV) exposure of the SU-8 in 20 second intervals.

Note: The images in Figures 5.1-5.4 have a yellow hue due to the type of light used in the lithography room of the NFSL. Yellow light is used in this room to avoid the UV spectrum and prevent the premature curing of SU-8 while working in the lab.

The above process was modified to work around temperature constraints imposed by the composite panel. Initially, the hard-bake step involved exposing the sample to 150°C for 30 minutes, which resulted in the delamination of the layers during our trial tests. Therefore, the baking steps for SU-8 were done at lower acceptable temperatures for a longer period of time. These steps are necessary to stabilize the SU-8 at the point of highest expected temperature.

It was mentioned earlier in Chapter 3 that due to the electrical insulation between the two aluminum facesheets of the composite, the ground of the antenna needs to be connected to the surface that the SU-8 is deposited on. The design solution to address this challenge is to use a tape mask during the SU-8 deposition process in order to leave a small area of the ground plane exposed for soldering purposes. This is demonstrated in step 2 of the process described above.

Through this process a substrate was successfully deposited on top of the hybrid panel without the need for adhesion promoters. Measuring the resulting thickness of the substrate shows edge beading effects where it is slightly thicker towards the edge of the panel. This is due to the spinning step in the deposition process that pushes the material outward to the edges. Using a caliper, it was measured that the substrate thickness is roughly 0.85mm at the center and 1.1mm around the edges. The relative smoothness of the SU-8 surface helps avoid rippling of the copper deposition in the next section. With regard to the overall size of the panel, the edge beading area is small enough that it does not affect the microstrip antenna elements located at the center. Simulating different variations of edge beading show that it does not cause any shifts in the operating frequency and does not introduce detrimental reflection losses to the antenna system.

The feed design for the antenna was changed from probe-fed in Chapter 4 to a co-planar inset feed. This design helps simplify the manufacturing process by restricting the entire antenna to one plane and removing the need for impedance matching at 50Ω. Modifying the simulation model to reflect all the changes is necessary in order to proceed to the next step and achieve accurate results. Figure 5.5 below shows the updated simulation model that includes the co-planar inset feed, edge beading effects, tape mask,

and ground connection. The antenna dimensions were then optimized for radiation performance and the extracted properties are listed in Table 5.1.

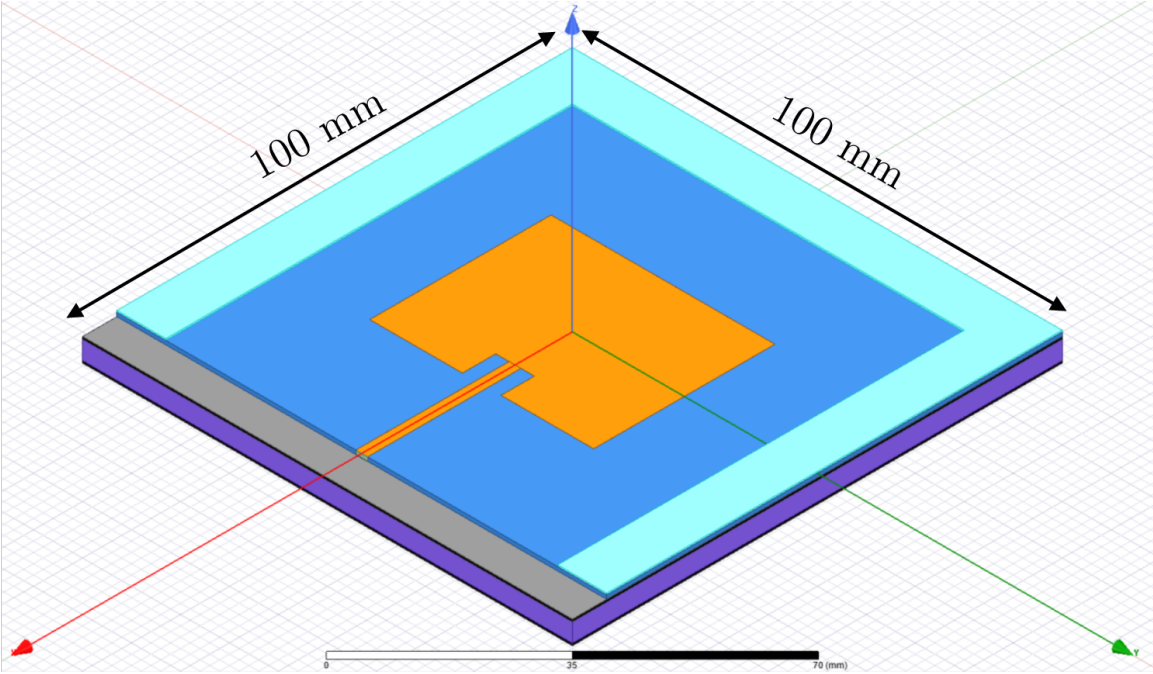

Figure 5.5: The updated simulation model of a patch antenna with inset feed, edge beading effects, tape mask and ground connection.

Table 5.1: Radiation properties of a single patch antenna element.

Parameter	Value	Unit
Center Frequency	2.25	GHz
10dB Bandwidth	40	MHz
Reflection Coefficient	-37.14	dB
Peak Gain	2.24	dB
Half-Power Beamwidth	82	degrees

The slight decrease in gain performance from the simulations in Chapter 4 stem from the decrease in substrate height and additional loss introduced by the inset feed, which is less ideal than a direct probe feed.

5.4 Copper Sputtering

The method used for depositing the copper elements onto the panel is called physical vapour deposition (PVD) or sputtering [89]. PVD produces a copper vapour at the atomic level using Argon gas and an arc source, which then condenses copper into a thin film on top of a substrate inside a vacuum chamber (Figure 5.6). PVD can create thin films deposited uniformly throughout, with a resolution of 10 nm.

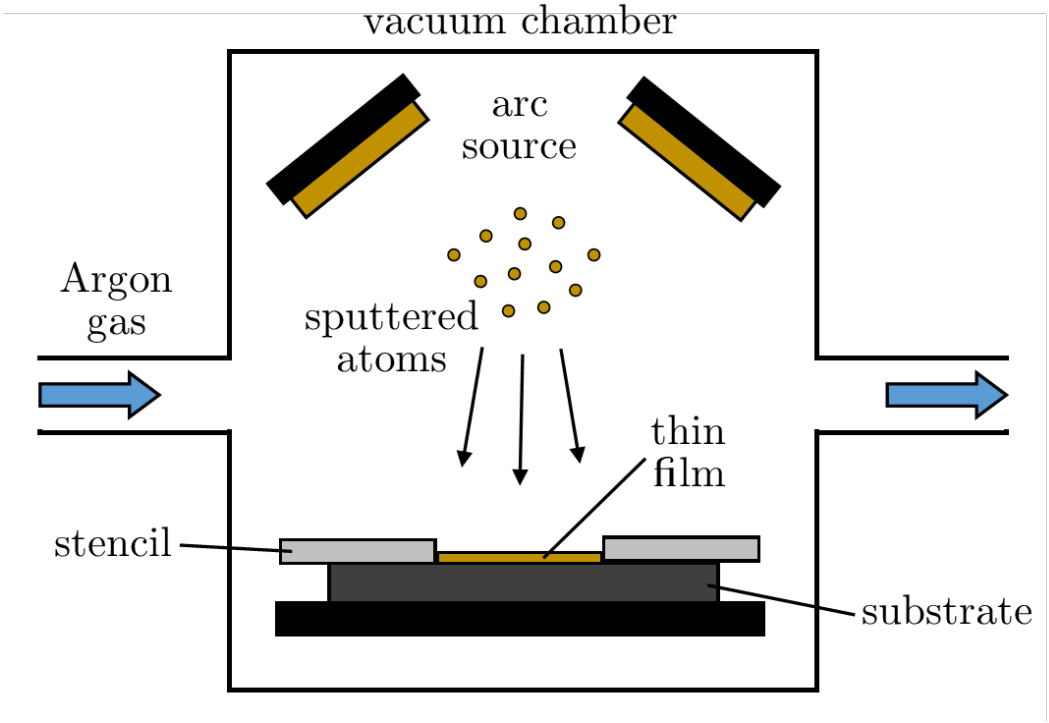

Figure 5.6: PVD by sputtering a copper vapour from an arc source to form a thin film of copper onto the substrate, shaped by an aluminum stencil.

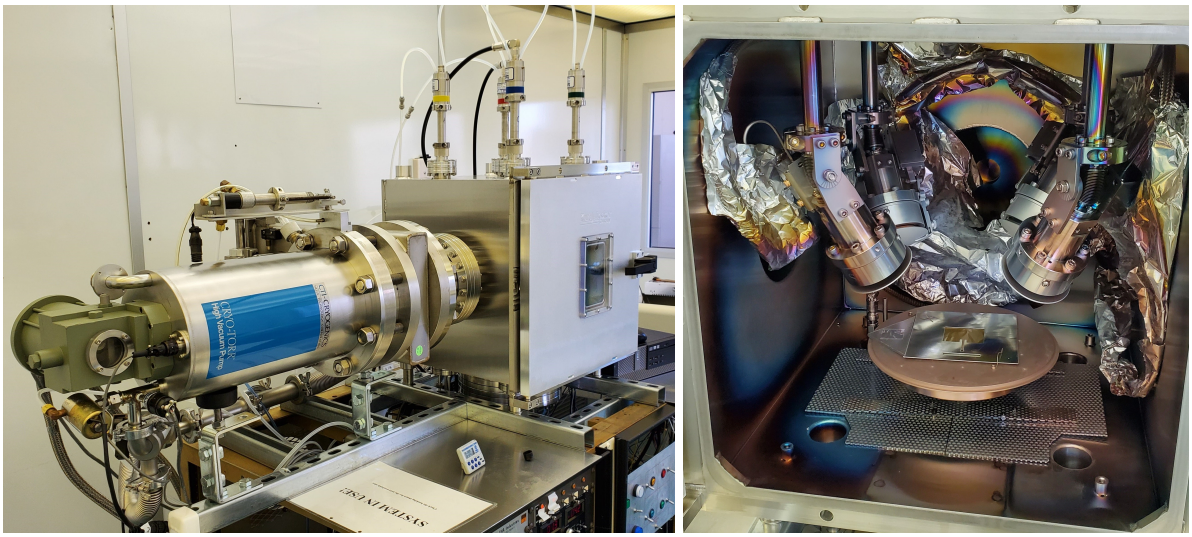

(a) (b)

Figure 5.7: Copper sputtering machine in the NFSL (a) outside and (b) inside the vacuum chamber.

The skin depth describes the area within the outer edges of a conducting material where most of the current density is concentrated. The thickness or distance of the skin depth defines where the current density falls to e^{-1} of the magnitude at the surface, and is dependent on the resistivity of the material and frequency of the excitation. Using equation (5.1), the skin depth (δ) of copper with resistivity $\rho = 1.7$ $\mu\Omega$ cm, a relative permeability of $\mu_r = 0.99$ and free space permeability $\mu_0 = 4\pi \times 10^{-7}$ at $f = 2.25$ GHz is around 1.37 μm. Therefore, the thickness of the copper antenna elements must be at least 1.37 μm. The copper layer for the patch antenna is designed to be 2μm thick.

$$\delta = \sqrt{\frac{\rho}{\pi f \mu_r \mu_0}} \tag{5.1}$$

A thin base layer of titanium (≈150 nm) is sputtered first to improve copper adhesion and support soldering connections. Afterwards, a 2μm layer of copper is sputtered on top. The duration of the sputtering process controls the thickness of the deposited film, which were previously determined by the NFSL through experimentation. Due to the thermal limitations of the hybrid composite, the process is paused for a 5 minute break after every 15 minutes.

In order to shape the deposited copper into the microstrip antenna and feed design, an aluminum stencil

is used to mask the substrate. The stencil is made to be slightly larger (12cm x 12cm) than the area of the composite panel (10cm x 10cm) and with a thickness of 0.02 inches. The shape is cut out of the aluminum sheet using a water jet to avoid burring and minimize any shadowing effects of the stencil. Sputtering is then used with the stencil mask (Figure 5.8) to deposit the microstrip antenna and feed line.

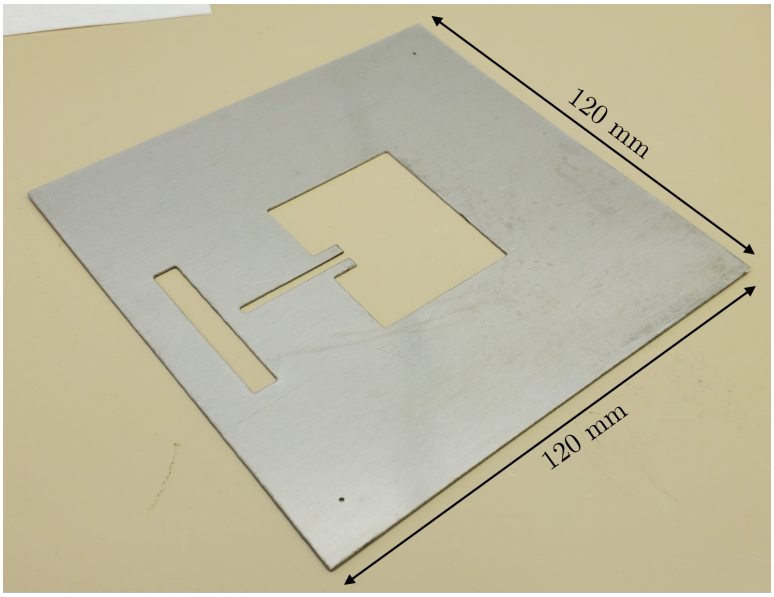

Figure 5.8: Stencil mask for the patch antenna, feed line, and soldering pad made from aluminum.

Two 1mm holes are added to the diagonal corners of the mask to align the composite panel corners below and center the antenna. The stencil has a rectangular area for a soldering pad on the exposed aluminum of the composite. The stencil is placed directly on top of the substrate and held down with tension from wires as shown in Figure 5.9. After sputtering, the mask is removed and the resulting antenna is shown in figure 5.10.

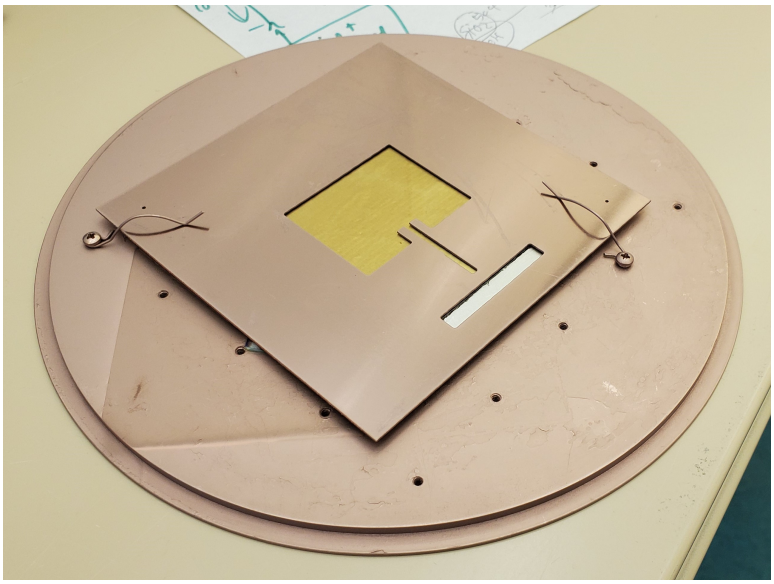

Figure 5.9: Stencil mask placed on top of the composite panel with SU-8, held down with wire holders.

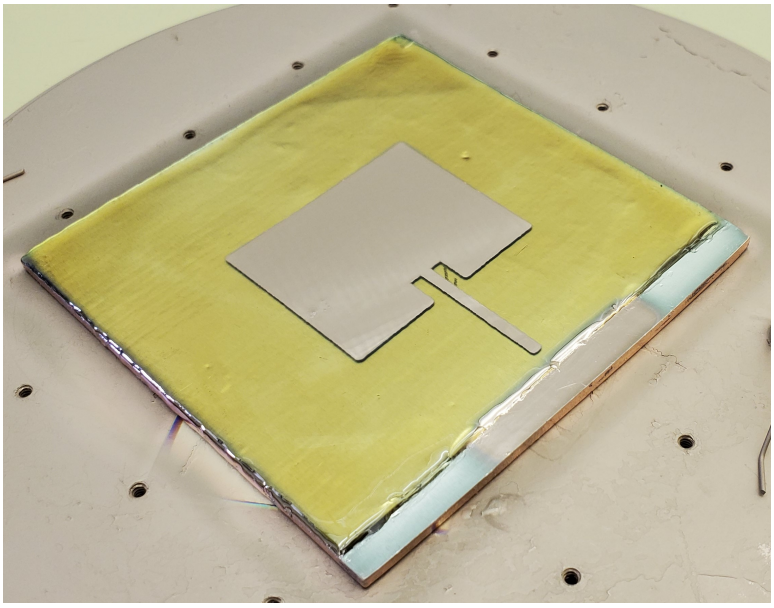

Figure 5.10: Microstrip patch antenna successfully deposited on top of composite panel and SU-8 substrate through copper sputtering.

Throughout the entire manufacturing process, a control antenna is also fabricated on top of a 1mm-thick aluminum alloy sheet. This panel has undergone exactly the same steps, albeit the absence of critical temperature limits suchlike those of the composite. The dimensions, connector, and grounding method is also kept identical. The control antenna will be used for comparison to the performance of the composite

panel antenna in the next chapter.

5.5 Conclusions

The SU-8 antenna manufacturing process has a comparable level of complexity and involvement as composite manufacturing. While temperature restrictions must be observed, the SU-8 antenna process is not constrained by pressure requirements such as in the hybrid composite manufacturing method [17], that includes low- and high-pressure stages. Furthermore, this method lends itself to increased adaptability to any shape or surface for antenna deposition. SU-8's excellent adhesion to inorganic materials also allows for the exclusion of other adhesives or fasteners. And finally, different antenna dimensions can also be realized by using different stencils constructed from aluminum while keeping the exact same process.

Overall, the antenna fabrication can be added as a final step to the standard composite manufacturing, creating a readily available communications component for general use. The work in this chapter verifies hypothesis 1, stating the microstrip antennas can be successfully deposited onto composite materials.

Chapter 6

Antenna Testing and Results

The performance of the prototype MFS antenna was evaluated through radiation tests at the University of Manitoba Antennas and Microwave Laboratory. This chapter discusses the test set-up, measurement methods, and results in comparison with the expectations from Chapter 4. These tests measured the S-parameters and radiation pattern of the antenna, from which I extracted properties such as operational frequency, reflection coefficient, bandwidth, peak gain and half-power beamwidth.

6.1 Test Equipment and Set-Up

The test equipment used for the following performance tests include the Keysight N5224B VNA (figure 3.3a) mentioned previously in Chapter 3 and the Satimo StarLab (figure 6.1). The resulting plots from these tests were compared with the plots shown in chapter 4 and re-evaluated for their potential uses.

The VNA test set-up has a 50-Ohm measurement interface that excites the device under test (DUT) and measures the resulting S-parameters. Before the test measurements were performed, the VNA was calibrated using a standard calibration test set including short, open, and matched loads. For a single-port device such as an antenna, the S-parameter (S_{11}) represents the reflection coefficient, which measures the ratio of incident power that is reflected back to the source. The S_{11} plot in the frequency domain illustrates the frequency at which the antenna transmits signals, the power efficiency, and the bandwidth capability.

The Satimo StarLab is a multi-probe system that measures the near-field radiation and then calculates the far-field radiation characteristics of the DUT. Before the test measurements were performed, the StarLab was calibrated using a standard horn antenna with a known gain, and the results were used to establish the performance of the DUT. The DUT was placed at the center and attached to a source that excited the antenna at the operating frequency (see Figure 6.2). The resulting emissions of the antenna were measured by the receivers that formed a circle around it and captured a single planar snapshot. The DUT is then rotated and measured again in 3° increments to be combined into a comprehensive radiation pattern. From these results, the peak gain was determined, which is one of the important parameters that describe antenna performance. Along with the gain, the half-power beamwidth was measured and illustrates how much of the radiation power is concentrated towards a single direction, which in this case, is the boresight of the antenna. The DUT is excited using a similar 50-Ohm measurement probe with a 6 dB attenuator that is calibrated into the system before measurement. Foam is placed around the source connector (as seen in Figure 6.2) to minimize effects of reflection.

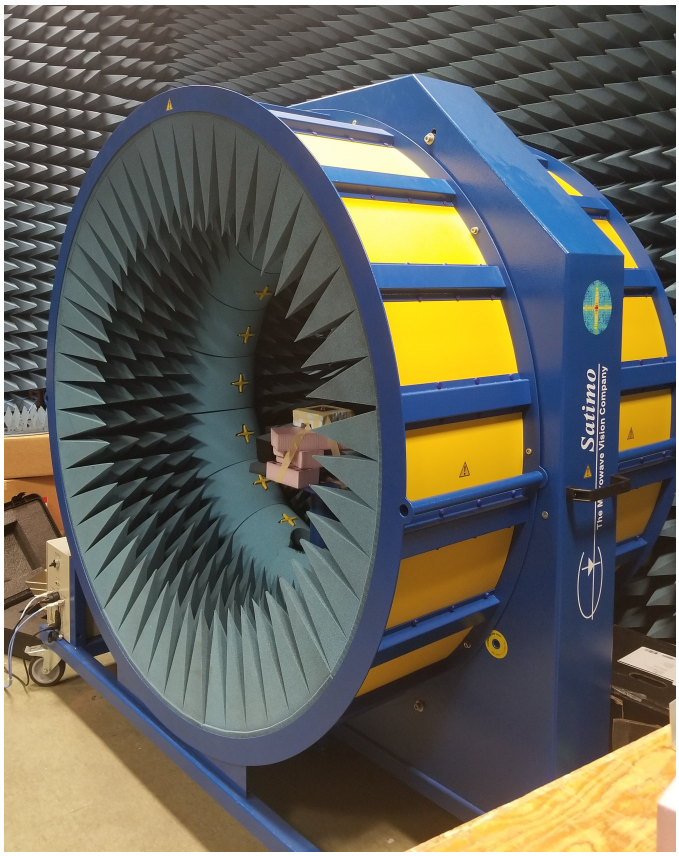

Figure 6.1: Satimo StarLab test set-up measuring the far-field radiation pattern of the prototype MFS antenna.

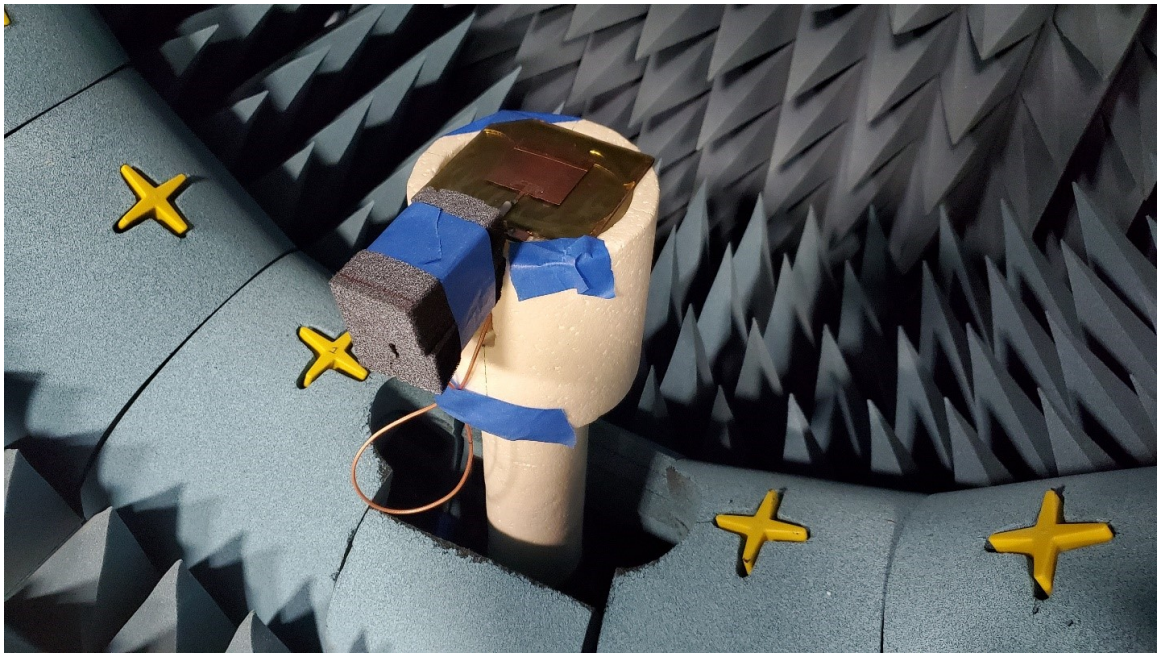

Figure 6.2: SU8-Composite patch antenna prototype mounted inside the Satimo StarLab test-setup.

6.2 Performance Evaluation

In order to analyze the potential of the prototype antenna for different applications, its properties were evaluated with design requirements. The gain dictates the ability of the transmitted signals to propagate across vast distances and various loss mechanisms. To demonstrate the improvement of a patch antenna over the commonly used dipole, the gain should be higher than the idealized dipole gain of about 2.15 dB [15].

The antenna bandwidth determines the data rate capability of communications, and therefore the volume of data transmitted over a period of time. Using the simple Nyquist criterion in equation 4.5 for a binary signal (M=2) and the minimum acceptable bit rate standard for amateur radio communication for basic telemetry (C=1200 bits per second), the bandwidth must be at least 1.2 kHz.

To ensure that the antenna maintains power efficiency, the reflection coefficient of the antenna at the desired operational frequency must be below -10dB. This threshold allows us to utilize at least 68% of the incident power for radiation, with about 32% loss. Minimizing this loss also helps any signals propagate further distances. An impedance mismatch at the antenna feed reduces the received power by a factor of the mismatch loss [90]. The mismatch loss is calculated using equation 6.1 below, where Γ is the linear reflection coefficient.

$$L_{mismatch}\ [\text{dB}] \ = -10\log_{10}(1-|\Gamma|^2) \tag{6.1}$$

The half-power beamwidth of the antenna has a reciprocal relationship with the required pointing accuracy of a spacecraft. While it is quite beneficial to concentrate the signal along one direction for efficiency, this poses stricter requirements for spacecraft to accurately control its orientation. A directive antenna such as this prototype has potential for missions with high pointing accuracy requirements such as nadir-pointing earth observation satellites.

The radiation properties of the antenna can be compared with microstrip patch antenna designs touched upon in the literature review. Table 6.1 below outlines the volume, gain, and features of each design.

Table 6.1: Comparison of some references from the literature review highlighting their volume, gain, frequency, and design features.

Reference	Volume [cm^3]	Gain [dBi]	Frequency Band	Design Features
Platero [this work]	10 x 10 x 0.56	1.45	S-band	MFS
Ferrero [25]	2.7 x 2.7 x 0.0892	6.2	S-band	quad-polarization
Chiu [27]	5.4 x 5.4 x 0.7	2.6	C-band	U-slot, folded patch
	4 x 4 x 0.7	2.4	S-C band	L-slit, folded patch
Malekpoor [29]	1.8 x 1.5 x 0.7	3.9	S-C band	folded patch
Nascetti [30]	3.97 x 1.2 x 0.21	5.9	S-band	circular polarization
Son [68]	7 x 7 x 0.7	6.3	C-band	MFS, stacked-patch
You [69]	4.8 x 4.8 x 1.5	11.2	X-band	MFS, stacked-patch

Furthermore, in order to assess and isolate the effects of the composite structure from the antenna design, a control antenna was manufactured in parallel. The control antenna consists of a simple 1mm-thick aluminum ground plane, which underwent the exact same processes as the composite as outlined in Chapter 5. The two antennas have the exact same dimensions and antenna design, and will undergo the same tests. This practice will evaluate the benefits of using a hybrid composite structure versus the more commonly-used material for spacecraft structures (aluminum).

6.3 Test Results

The prototype antennas were first tested on the VNA for their reflection coefficients, and the resulting S_{11} frequency response plots are shown below in Figures 6.3-6.4. From these graphs, I extracted the central operating frequency for the composite antenna to be 2.44 GHz with a reflection coefficient of -17 dB and a -10 dB bandwidth of 60.5 MHz. Alternatively, the control (aluminum) antenna showed f = 2.20 GHz, S_{11} = -13 dB and bandwidth = 85 MHz.

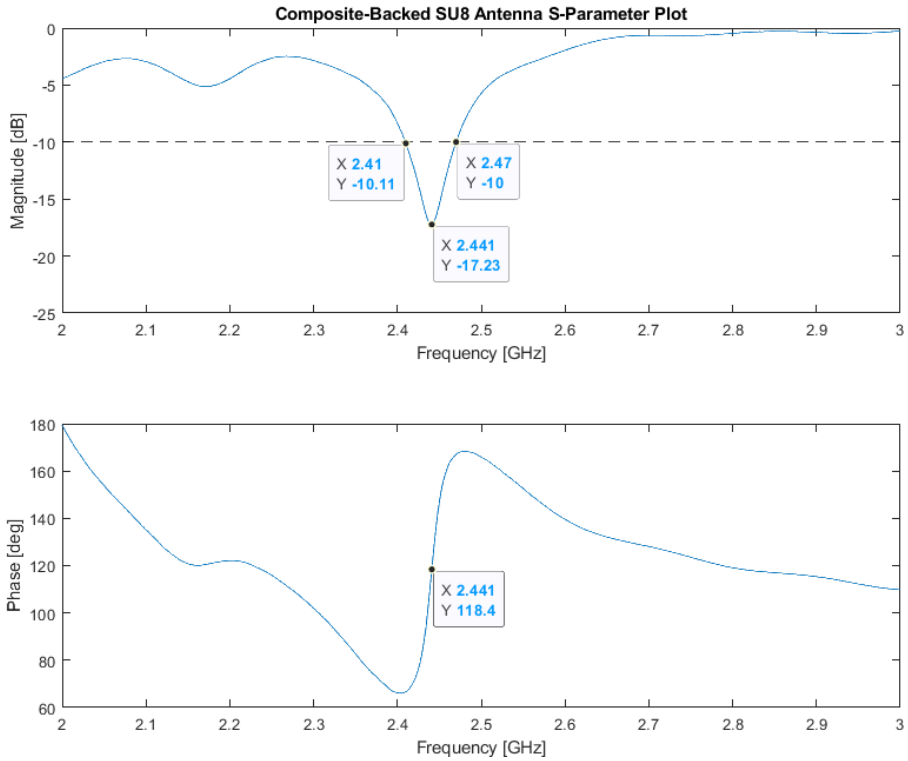

Figure 6.3: The measured reflection coefficient S_{11} frequency response for the hybrid composite antenna, showing center frequency and bandwidth.

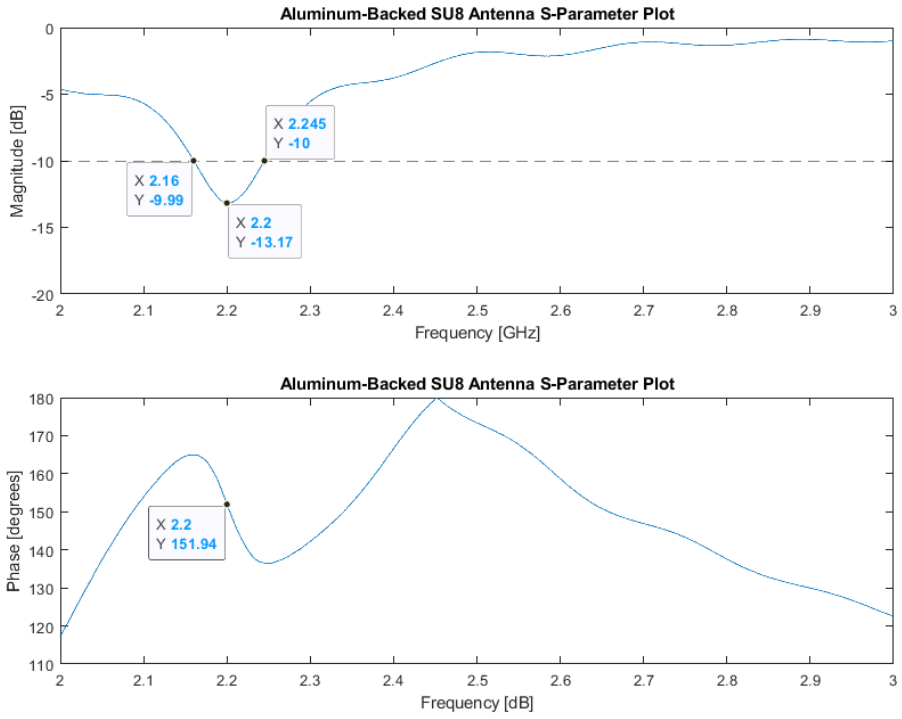

Figure 6.4: The measured reflection coefficient S_{11} frequency response for the control antenna on aluminum, showing center frequency and bandwidth.

Afterwards, the antennas were tested in the Satimo StarLab for their radiation patterns, and the resulting plots for gain in phi and theta are shown below in Figures 6.5-6.6. These figures show a peak gain of 1.37 dBi and a half power beamwidth of 90° at $\phi = 99°, \theta = 342°$ in the E_θ orientation at $f = 2.5$ GHz for the hybrid composite antenna. It can be seen that although the S-parameter plots for this antenna displayed a resonant frequency of 2.44 GHz (Figure 6.3), the peak gain of the antenna occurs when measured at 2.5 GHz instead. Alternatively, the control antenna demonstrates a peak gain of -2.27 dBi and half power beamwidth of 51° at $\phi = 0°$, $\theta = 9°$ in the E_ϕ orientation at $f = 2.2$ GHz.

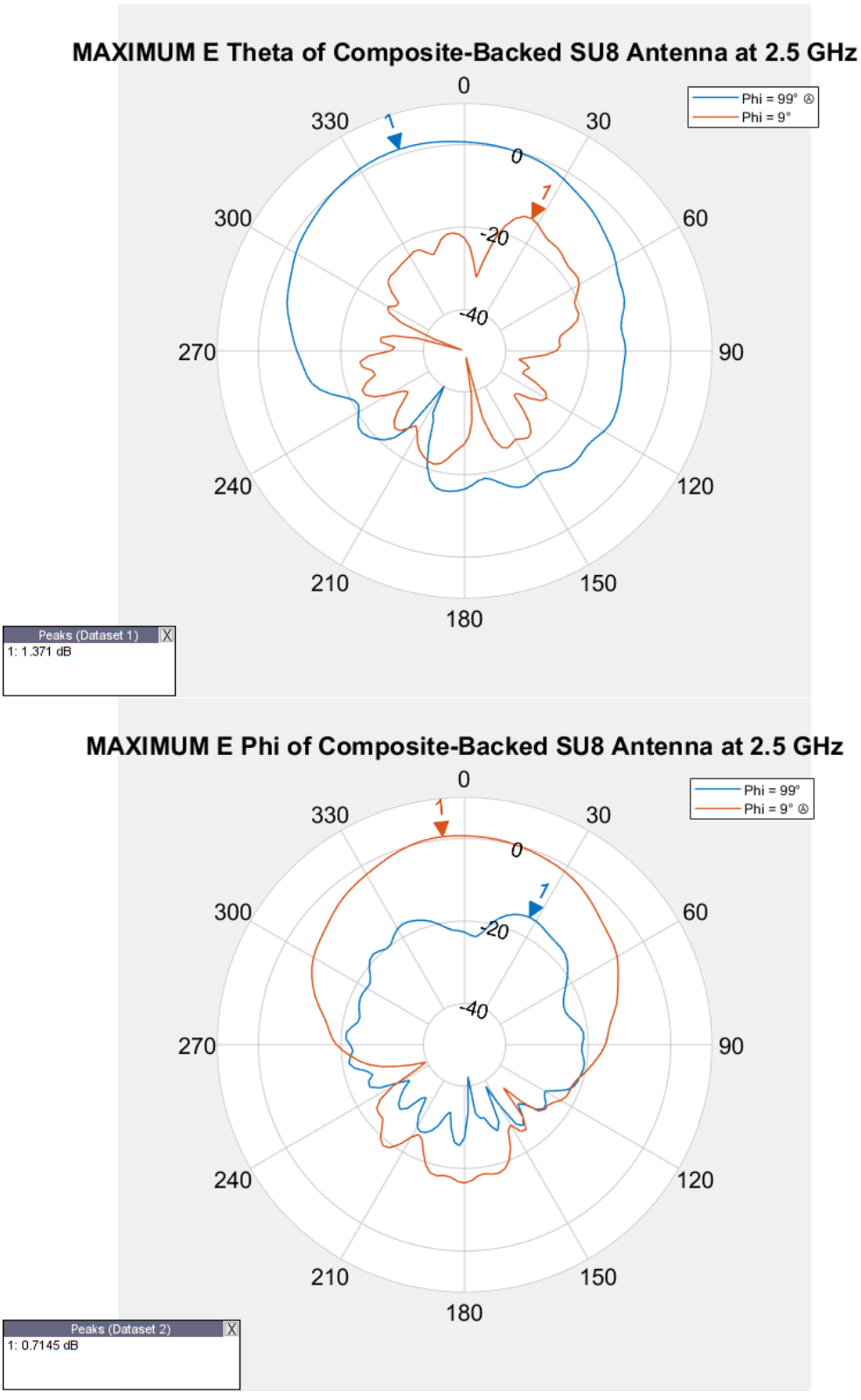

Figure 6.5: The measured radiation pattern of the hybrid composite antenna, showing realized gain.

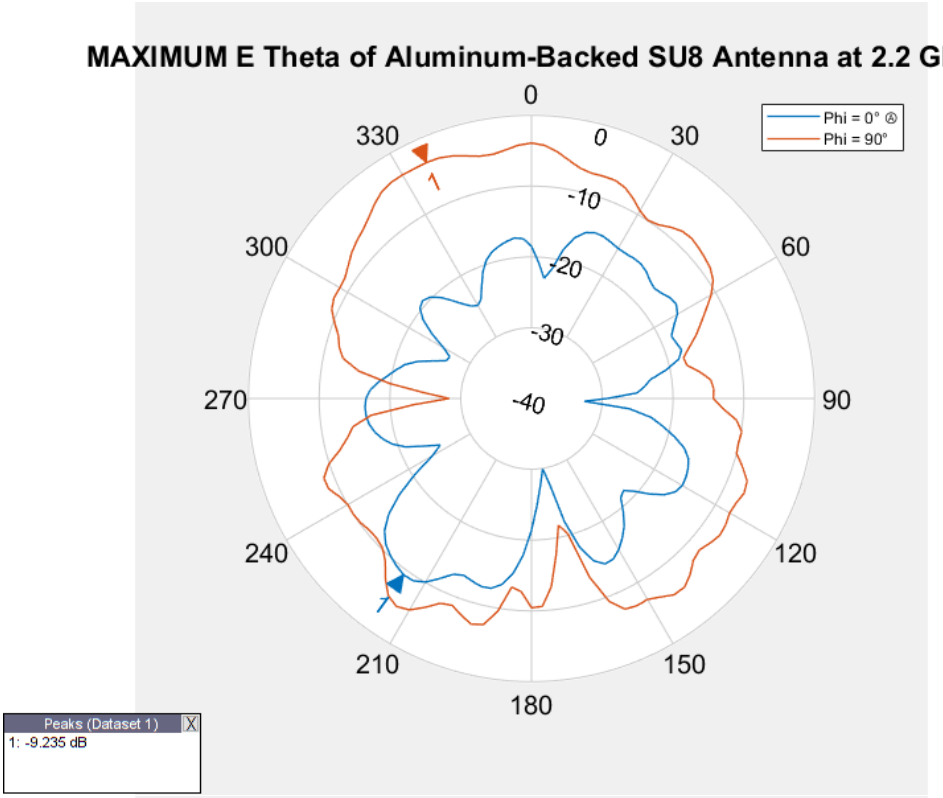

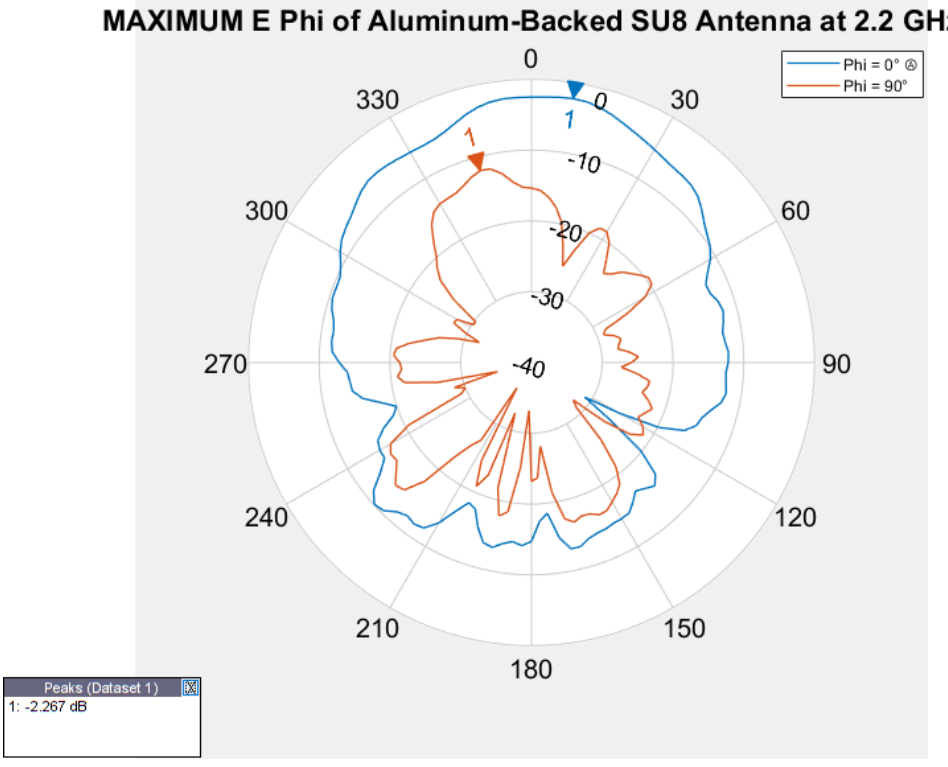

Figure 6.6: The measured radiation pattern of the control antenna on aluminum showing realized gain.

6.4 Discussion

The comparison between the simulated results from Table 5.1 and measured results are summarized below in Table 6.2, showing a decline of the properties from the expectations in Chapter 5. This discrepancy can be attributed to losses in the dielectric, connector, and manufacturing process. Further discussion of the discrepancy and the investigation that followed is described in Section 6.4.2

The mismatch loss and peak gain values in Table 6.2 are calculated from the lab-measured reflection coefficient and realized gain using equation 6.1. The realized gain takes into account the mismatch loss, and is therefore factored out in order to compare the peak gain performances.

Table 6.2: Summary of simulated/expected vs. measured radiation properties of a single patch antenna element with inline feed.

Parameter	Simulated Values	Control Antenna	Composite Antenna
Center Frequency	2.25 GHz	2.2 GHz	2.5 GHz
10dB Bandwidth	40 MHz	51 MHz	60.5 MHz
Reflection Coefficient	-37.14 dB	-13.17 dB	-17.23 dB
Mismatch Loss	0.0008 dB	0.215 dB	0.083 dB
Realized Gain	2.24 dBi	-2.27 dBi	1.37 dBi
Peak Gain	2.24 dBi	-2.06 dBi	1.45 dBi
Half-Power Beamwidth	82°	51°	90°

The resulting gain performance of the composite MFS antenna has shown to be lower than all of the patch antennas summarized in Table 6.1, and the dipole standard of 2.15 dB, with no improvement over an idealized dipole antenna gain. The measured bandwidth also provided a maximum data rate of up to 90 Mbps for a simple binary signal (M=2) using equation 4.5. Finally, the reflection coefficients were below -10dB, meeting the initial requirement, with a transmission power efficiency of about 78% and 86% for the control and composite antennas respectively. The results also showed an increase in gain from the control to the composite antenna, despite the fact that they have similar levels of reflection coefficient. Finally, the

peak gain of the composite MFS antenna was 0.79 dB lower than expected from the simulation results, which is above the acceptable level of error of approximately 0.5 dB, and therefore required further investigation. The investigation of the discrepancies and the loss mechanisms it can be attributed to are discussed in the following two sections.

6.4.1 Material Fragility and Antenna Repair

During the final steps of the fabrication process, a rapid temperature change caused cracking in the deposited SU-8 dielectric layer, and the fracture propagated across the prototype and the deposited copper layer. The damaged antenna prototype is shown in Figure 6.7 below.

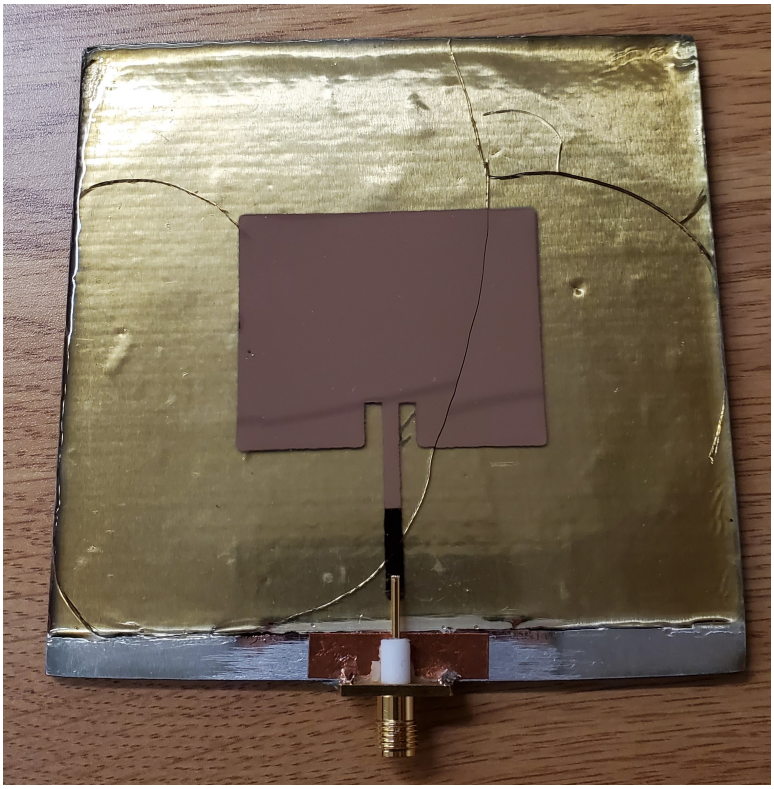

Figure 6.7: Damaged antenna prototype (10 cm x 10 cm) showing fractures across the dielectric layer and the sputtered copper layer.

The fractures in the SU-8 caused the dielectric layer to lose adhesion to the composite panel surface, even with minimal and gentle handling of the prototype. This initially created an air gap between the SU-8 and the ground plane at the center of the antenna, which gradually progressed to the edges. The fracture in the sputtered copper layer was repaired using adhesive copper tape, and eventually replaced with a patch of

copper tape with similar dimensions, and modified for impedance matching. The resulting prototype that was tested with the result outcome in Section 6.3 is shown in Figure 6.8. The effects of the cracked dielectric layer, such as the air gap and change in height, shifted the ideal patch dimensions for the antenna design, which necessitated modifications for optimization.

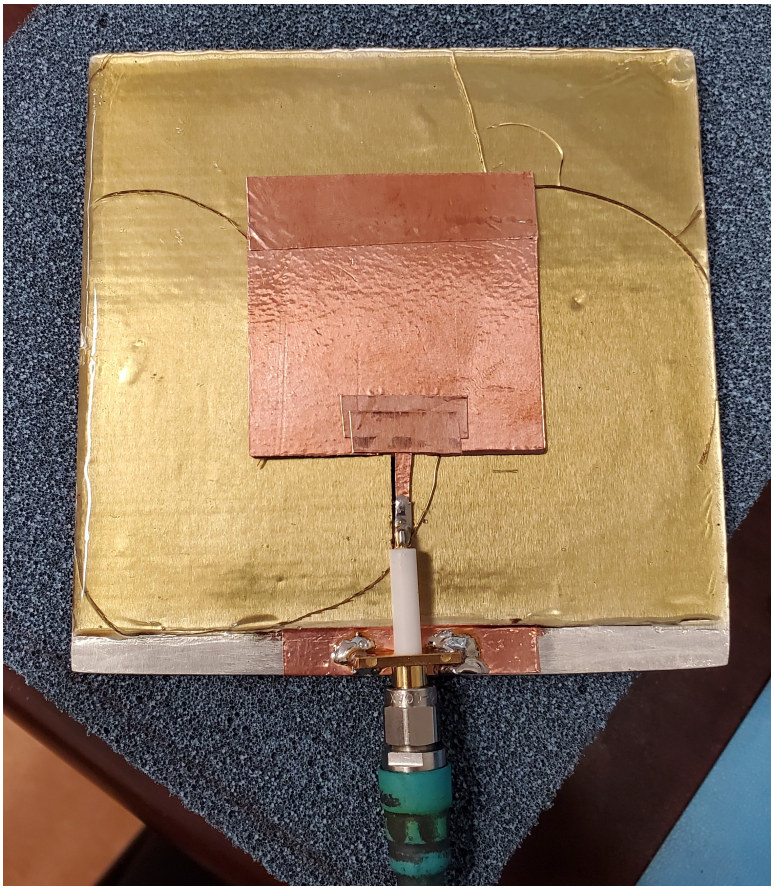

Figure 6.8: Repaired antenna prototype (10 cm x 10 cm) with adhesive copper tape, where the patch dimensions are modified to optimize impedance matching.

The prototype shown above in Figure 6.8 is the device under test with results presented in Section 6.3. Since the dimensions were modified from the design in Figure 5.5, the antenna was re-modelled in HFSS to account for the effects of the cracked SU8 layer. Details of the subsequent sensitivity analyses are presented in Appendix A. Although I could not pinpoint a single cracked dielectric model to fully represent the lab-measured antenna performance, the discrepancy can be attributed to a compounding of different loss mechanisms discussed in the following section.

6.4.2 Investigation of Loss Mechanisms

This section discusses the loss mechanisms that contributed to the discrepancy between expected, shown in Table 6.2, and measured peak gain of $\Delta G = 0.79$ dB. Among the various losses, dielectric loss and connector loss were considered to be the major contributors. Additionally, this section also provides a summary of the sensitivity analyses presented in Appendix A.

Manufacturing Tolerance

Some uncertainties were introduced into the antenna system stemming from the manufacturing process, such as the dielectric height and patch antenna dimensions. The antenna design, namely the resonant frequency of the antenna and the intrinsic impedance of the microstrip feed line, are highly dependent on these two properties. Changes in these properties can cause the resonant frequency to shift and create an impedance mismatch, and since patch antennas have very narrow bandwidths [15] (as seen in Figure 4.2), this shift causes significant decrease in radiation efficiency. Additionally, the intrinsic impedance of the microstrip antenna was very sensitive to these changes and therefore exacerbated the impedance mismatch.

Although the surface of the SU-8 layer is relatively smooth, edge beading effects from the deposition method created a height fluctuation from the centre to the edge. This effect was simplified and modelled in Section 5.3 and Figure 5.5, and despite the optimization, the model has limitations that do not fully represent the deposited layer. The simulations showed that a substrate height difference of $\Delta h = 0.1$ mm can cause a shift in the resonance frequency of up to 10 MHz and increase in S_{11} reflection coefficient of up to 18.5 dB.

Another source of manufacturing uncertainty is the deposition method of the copper layer. After the sputtering process, there was an observable bleedthrough of the copper material past the stencil and increased dimensions of up to 1 mm. Because the frequency response is sensitive to the patch antenna dimensions, the bleedthrough caused significant detriment to radiation performance. The simulations showed that an increase of 1 mm in all dimensions created a shift in the resonance frequency of up to 50 MHz and increase

in S_{11} reflection coefficient of up to 11.3 dB.

Dielectric Loss

The radiation efficiency of an antenna is directly related to the dielectric loss of the substrate material. The dielectric loss, or also expressed as the loss tangent, determines how much radiation energy is lost within the substrate, and is calculated using equation (3.3). Another uncertainty that stems from the manufacturing process of the antenna prototype is the dielectric permittivity of the SU-8 material.

The theoretical and measured values for the SU-8 properties in Table 3.4 reflect parameter values for a fully-cross linked SU-8 sample. Due to the modified deposition process that was used, these are likely not representative of the actual properties of the SU-8 layer of the antenna prototype. According to [78], the fabrication process for SU-8 is demonstrated to have a significant impact on the loss behaviour. The reduced temperature of the baking process can result in a partially cross-linked SU-8 layer, and therefore decrease the real permittivity and increase the complex permittivity (i.e. increasing the loss tangent). Using the same model equations as in Chapter 3 from [78], the complex dielectric permittivity of a partially cross-linked SU-8 substrate is $\varepsilon_r = 2.95 - j0.0905$ with a loss tangent of $\tan\delta = 0.0307$, which is double that of the fully cross-linked calculations.

There were also differences between the material under test in [78] used to determine the dielectric model and the material used for the MFS antenna prototype. The SU-8 tested in [78] used SU-8 2100 with thicknesses of 330 to 450 μm and measured at frequencies from 0.2 to 1 THz. On the other hand, the MFS antenna prototype used SU-8 2075 with a thickness ranging from 8000 to 1200 μm intended for use at 2.25 GHz. These minor differences between the SU-8 materials used in the dielectric model versus the realized prototype contribute to the discrepancy.

The addition of the air gap between the dielectric layer and the composite ground plane complicates the antenna system by creating a mixed-dielectric substrate. This further decreases the permittivity since

a weighted average between the two materials will be somewhere between $\varepsilon_{SU8} = 2.95$ and $\varepsilon_{air} = 1$. Furthermore, it also introduces a material interface between the SU-8 and air that can result in added loss. The height and shape of the air gap is another source of uncertainty as it can fluctuate while handling the prototype during testing, which ultimately resulted in the edges of the SU-8 layer losing adhesion.

Connector Loss

One of the biggest challenges in designing the MFS antenna was finding a suitable feeding method to excite the patch. Some common feeding methods for microstrip patch antennas were ruled out due to the layered structure of the hybrid composite material, wherein a non-conductive layer is sandwiched between partially (CFC) and fully (aluminum) conductive layers. Additionally, the SMA connector installation also posed an issue as most connectors are designed for antennas that have the ground plane as the bottom layer. In this case, the thin aluminum layer at the bottom of the composite is not connected to the antenna's ground plane (top aluminum layer) as seen in Figure 3.1.

The connector that was chosen for this antenna prototype is a 50 Ω panel mount SMA connector as seen in Figure 6.7 and Figure 6.8. This design was chosen due to the separation and protrusion of the center pin from the grounded connector housing, allowing it to reach the microstrip feed line past the exposed aluminum ground patch. This configuration was not the ideal use for this connector, but it was the most mechanically viable solution that works with the geometry of the antenna prototype. The ground connection was made by sanding off the anodized aluminum layer and placing a piece of copper tape on top, as seen in Figure 6.7 and Figure 6.8. The grounded connector receptacle is then soldered on the copper tape pad, since aluminum does not adhere to solder well.

Connector loss is another contributing factor to the low radiation efficiency of the antenna prototype. Due to the less-than-ideal configuration of the connector, the quality of the electrical connections come into question. In the case where there is a poor electrical connection, it can be assumed that some excitation is transferred through coupling of the center pin and feed line, with the center pin conductor also radiating.

In summary, the quality of the SMA's electrical connection is significantly detrimental to the radiation performance of the antenna.

Sensitivity Analysis

Due to the uncertainties mentioned above, I conducted several sensitivity analyses for the materials used in the antenna prototype. Details on the simulation analyses are presented in Appendix A. In summary, variations in the dielectric permittivity and dielectric height (edge beading effects) showed shifts in the resonant frequency and increase in reflection coefficient. On the other hand, copper and aluminum sensitivity analyses showed little to no effects on the radiation performance of the antenna simulation.

Table 6.3: Summary of the material sensitivity analyses performed on the hybrid composite antenna model on HFSS.

Variable parameter	Variable swing	Max ΔS_{11} [dB]
Dielectric permittivity	$\pm 10\%$	19.8
Dielectric height	± 2 mm	27.4
Copper conductivity	$\pm 10\%$	17.3
Aluminum conductivity	-90% to -40%	no effect

Modelling Limitations

Overall, there were limitations in the model fidelity that likely contributed to the observed discrepancies between simulation and test results. These modelling limitations prevented complete material representation, such as the uncertainties discussed in this section. Complicating this, were the complexities of the carbon fibre composite, which contained a mixture of conductive rods and non-conductive material. This potentially introduced parasitic behaviour at higher frequencies beyond the characterization test range. I lacked the sub-surface construction geometry and dimensions to support a realistic internal model of the structure. In addition, modelling the intricacies of the manufacturing process would have required meticulous deconstruction and microscopic analysis, which was beyond the scope of this study.

Testing Limitations

Another possible source of error that factors into the discrepancy were the limitations imposed on the testing of the antenna. Proper alignment of the DUT within the Satimo StarLab is necessary for obtaining accurate measurements. There is some slight error in the positioning of the antenna within the measurement facility, and since measurements are taken every 3°, there is the possibility that the maximum gain point was not measured. Additionally, there were limitations on the number of measurement iterations I could perform due to restricted facility access during the pandemic.

6.5 Conclusions

In summary, this chapter presented the measured lab results for the prototype antenna that showed a deviation in radiation performance from the expectations in Chapter 5. The results summarized in Table 6.2 show a discrepancy in the centre frequency by 0.250 GHz and the peak gain of 0.79 dB, which is beyond an acceptable error or discrepancy. This difference can be attributed to a compounding of various loss mechanisms present in the as-built prototype antenna, most specifically the damage from the cracking of the dielectric layer. Other sources of losses that were investigated include manufacturing tolerances, dielectric loss, connector loss, material sensitivity, and modelling and testing limitations. The combination of all the mechanisms discussed in this chapter account for the performance discrepancy. Future work for this project, such as another manufacturing iteration with a different connector, would resolve this difference and is discussed in the next chapter.

Chapter 7

Conclusions

7.1 Summary of Research

This thesis presented the design, fabrication, and feasibility of embedded microstrip antennas within composite materials that created a multifunctional structure. This component was a proposed solution for volume efficiency, mass reduction, improved access to space, ease of integration, and adaptable communications parts. Through this research I have provided material properties, case studies, manufacturing methods, simulation analyses, and experimental results.

I characterized materials such as carbon fibre composites (CFC), polyethylene fibre composites (PFC), and SU-8 photoresist for their RF properties. Using this information, a microstrip patch antenna was designed and simulated in HFSS to analyze the radiation performance and its applications for different types of space missions. A novel manufacturing process was then developed to realize the antenna design while maintaining structural benefits of the composite structure. Finally, I presented the test results of a prototype antenna, evaluated the feasibility of the overall MFS component as a communications solution, and provided investigation analyses.

7.2 Research Goals

The goal of this research project was to develop a multifunctional structure that can transmit and receive communication signals. By furthering the field of MFS and spacecraft miniaturization, I sought to improve space accessibility by making space missions more affordable, efficient, and less risky. I presented an analysis of the feasibility of a novel MFS antenna through simulations and prototype testing. The methods and tests performed in this thesis were used to verify four hypotheses that were expected of this research.

Hypothesis 1 stated that microstrip antennas can be successfully deposited onto composite materials. The utilization of SU-8 material and copper sputtering for the dielectric and microstrip components initially demonstrated successful deposition onto the hybrid composite panel, but was not resilient against temperature changes and handling over time. Although the previous chapter showed that SU-8 and the hybrid composite were not an ideal pair, polymer deposition and copper sputtering still have much potential for this application. The polymer deposition method is adaptable for different substrate shapes, and the sputtering process allows the deposition of copper in any design through the use of reusable stencil masks.

Hypothesis 2 stated that CFRP can be incorporated into the MFS without detriment to antenna performance. The CFRP showed undesirable anisotropic electrical properties, but using a hybrid composite with aluminum proved advantageous to provide an isotropic ground plane while maintaining the lightweight and structural benefits of composite materials. Although the radiation performance was less than expected from the simulation, the MFS antenna prototype still exhibited patch antenna behaviour within the S-band range. This was verified through simulation and experimental results showing the radiation performance of the MFS antenna.

Hypothesis 3 stated that the MFS antenna meets the performance standards for satellite communications. Simulation results and case studies of the design show potential applications for both small and large spacecraft's tracking, telemetry and command communications. Unfortunately, the radiation performance of the realized antenna prototype did not meet the minimum criteria to be deemed more advantageous over

other antenna solutions. Therefore, further work is recommended such as more manufacturing iterations, improving fabrication tolerances, and investigation of other dielectric materials and feed connectors.

Hypothesis 4 stated that the MFS antenna can reduce the component footprint and maximize useable spacecraft volume. Compared to protruding dipole or monopole antennas and high gain reflectors, the MFS antenna structure has a reduced footprint. The flat profile and elimination of any deployable mechanisms allow for integration onto surfaces which increases available satellite space for valuable bus and payload instruments. A reduced volume and non-protruding antenna also reduces the risks in the communications system from either deployment failure or debris collision. Due to the low gain performance of the antenna, larger arrays would have to be implemented to meet minimum mission requirements. This would reduce the benefits and deem it non-ideal for small satellites, but still have potential for larger spacecraft.

7.3 Contributions

My research aimed to further the field of spacecraft miniaturization and multifunctional structures by embedding antennas within composite structures. A summary of the research contributions of this thesis are as follows:

1. **Utilization and characterization of hybrid composite materials and SU-8 photoresist**

   Composite materials provide lightweight and durable structures, and while usually characterized for their mechanical properties, are not typically discussed with regards to their electrical properties. In addition, dielectric spectrometer results for SU-8 are also provided.

2. **Application of SU-8 as an antenna dielectric**

   SU-8 is not a commonly used dielectric material for microstrip patch antennas. This research presented a design, fabrication method, experimental results, and an evaluation of the performance of such an antenna.

3. **Novel manufacturing method for a MFS antenna**

The combination of the hybrid composite with the SU-8 antenna required careful integration of the manufacturing method to work within constraints of the composite. Pre-existing methods of SU-8 and copper deposition were modified to accommodate lower temperature limits.

4. **Reduced MMOD and deployment risks**

   While these risks are posed to more popular antenna solutions, the flat profile of the MFS patch antenna precludes them. Reducing the safety-critical nature of space missions can help improve space accessibility for more institutions.

5. **Spatial effciency**

   Embedded functional components within the structure can maximize volume within the spacecraft for other instruments or enable spacecraft miniaturization. Especially on small spacecraft missions, space is a limited resource and extra space can add value by allowing more payload instruments.

7.4 Future Work

This research demonstrated a single-element MFS patch antenna design that has potential to be expanded and built upon. Future work on this research project includes investigating other polymer materials that would be more suitable for use with the hybrid composite material. The effects of the curing processes and temperatures on the electrical and RF properties of different polymer materials can also be studied for compatibility. Additionally, other feeding methods can also be explored such as probe feeding and aperture coupling. Mechanical analyses should also be performed to evaluate the fragility and resilience of future prototypes.

Other future work improvements involve gain and polarization optimization, array prototyping, and integrated electronic beam steering. Gain improvement and addition of other polarization configurations can be realized through design techniques that were explored in the literature review. These added features should be implemented to balance the complexity of the design to the manufacturing feasibility. The single element design can be duplicated and configured into a planar array that can also improve the gain significantly and

achieve circular polarization in certain configurations. And finally, electronic beamsteering can be implemented with the use of embedded microstrip devices. This feature will likely add to the complexity of design and pose a challenge as to where the added circuitry can be embedded and located.

7.5 Closing Remarks

This research provided the foundation for multifunctional embedded patch antennas for small and large satellite communications. A novel design and manufacturing process were introduced that helped maximize spacecraft volume, reduce mass, and increase reliability. These advantages factored into contributions to the effort of spacecraft miniaturization and improved access to space. While the prototype showed non-ideal radiation performance for spacecraft antennas, the potential for future work and expansion of this research field still show beneficial applications to a wide range of space missions. This research established a promising approach to designing and manufacturing satellite antennas that electrically characterized innovative materials and developed novel manufacturing techniques.

Appendix A

Simulation Sensitivity Analyses

Due to the discrepancy between expected and lab-measured results, and the various uncertainties introduced by the manufacturing process, I conducted material sensitivity analysis simulations in HFSS. The purpose of these analyses is to find the possible sources of losses that contribute to the overall low efficiency of the antenna. In order to isolate each of the effects, the simulation analyses were performed on the model from chapter 5, figure 5.5.

A.1 Dielectric Permittivity

To study the effects of variations in the SU-8 dielectric constant (epsilon), I performed simulations of the antenna while shifting the epsilon value $\pm 5\%$ and $\pm 10\%$. The results are summarized in Table A.1 and the S11 frequency response in Figure A.1. The results show that varying the dielectric constant at these margins cause a very small shift in the center frequency and reflection coefficient. Although these differences are still significantly different from the measured lab results. An increase in epsilon shows an approximately linear decrease in center frequency, and a $\pm 5\%$ variation in epsilon shows an averaged increase in S_{11} of approximately 14 dB.

Table A.1: Simulation results for various values of dielectric permittivity shifted ±5% and ±10% from the nominal value

Epsilon	Δ Epsilon	Center Frequency [GHz]	S_{11} [dB]
2.925	-10%	2.31	-32.6
3.0875	-5%	2.25	-38.1
3.25	0%	2.20	-50.5
3.4125	+5%	2.15	-34.5
3.575	+10%	2.10	-30.7

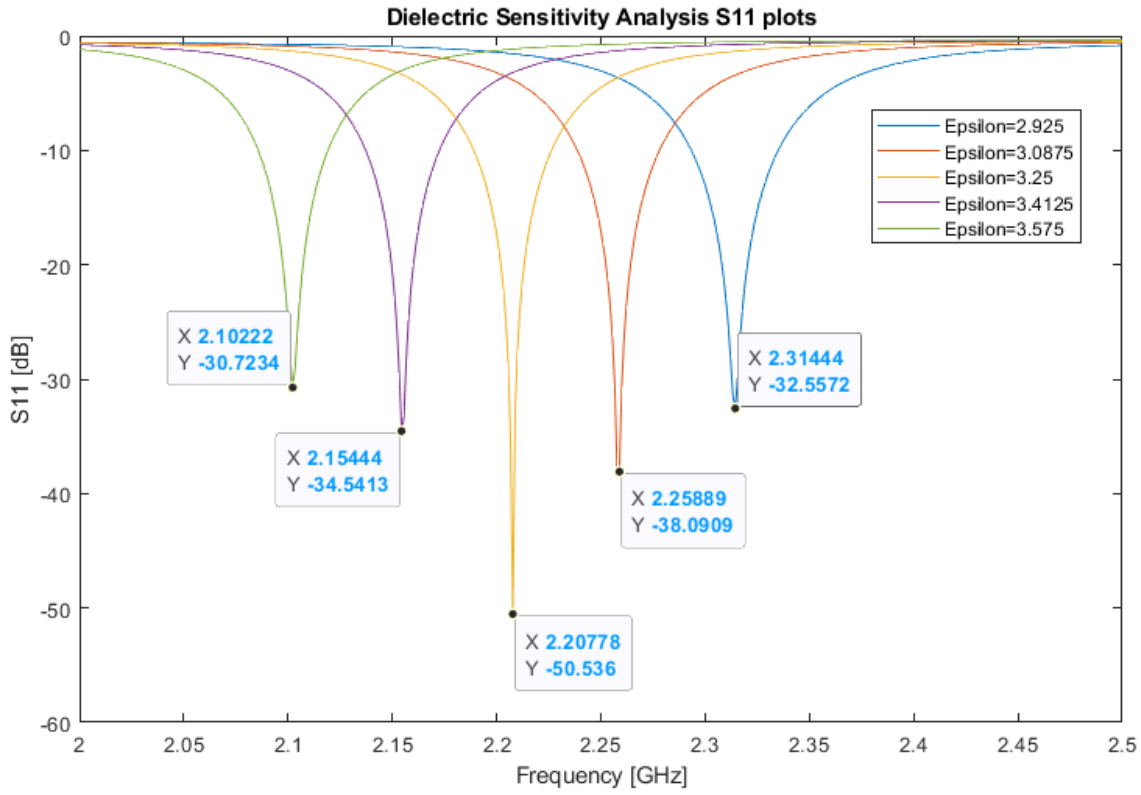

Figure A.1: S11 plot for various values of dielectric permittivity shifted ±5% and ±10% from the nominal value

A.2 Dielectric Height

This simulation analysis investigates the effect of the height difference between the center and the edges of the SU-8 dielectric. Starting with an ideal flat 1 mm substrate, the height differential is increased by 0.2 mm. The results are summarized in Table A.2 and the S11 frequency response in Figure A.2. Note that the simulation model was optimized for the case of center height = 0.8 mm and edge height = 1.2 mm. The results show that compared to the previous section, there is a smaller shift in frequency shift but a larger increase in reflection coefficient (S_{11}).

Table A.2: Simulation results for various height differentials between the center and the edge of the SU-8 substrate

Center height [mm]	Edge height [mm]	Δheight [mm]	Center Frequency [GHz]	S_{11} [dB]
1	1	0	2.19	-20.6
0.9	1.1	0.2	2.20	-25.0
0.8	1.2	0.4	2.21	-44.8
0.7	1.3	0.6	2.21	-24.7
0.6	1.4	0.8	2.22	-17.4

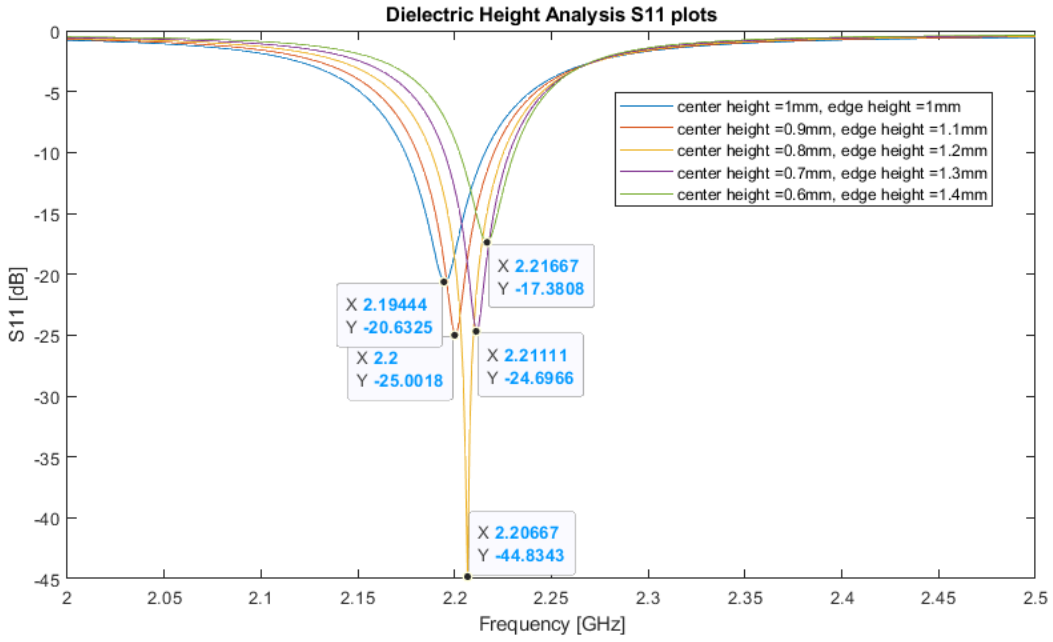

Figure A.2: S11 plot for various height differentials between the center and the edge of the SU-8 substrate

A.3 Copper and Aluminum Conductivity

This simulation investigates the effect of the conductivity of metals in the antenna prototype on the radiation efficiency. In a similar fashion, the conductivity of the copper layer was varied by ±5% and ±10% from the nominal value of 58 000 000 S/m. The results in Table A.3 show that the change in copper conductivity have little to no effect on the resonant frequency and reflection coefficient.

Table A.3: Simulation results for various values of copper conductivity shifted ±5% and ±10% from the nominal value

Conductivity [S/m]	Δ Conductivity	Center Frequency [GHz]	S_{11} [dB]
52 200 000	-10%	2.21	-57.1
55 100 000	-5%	2.21	-46.0
58 000 000	0%	2.21	-39.8
60 900 000	+5%	2.21	-41.1
63 800 000	+10%	2.21	-44.1

The thin aluminum film used in the hybrid composite material is Al 1100, which has a conductivity of approximately 33 000 000 S/m or 57% IACS (International Annealed Copper Standard = 58 000 000 S/m). In the simulation, I varied the aluminum conductivity from 10% to 60% and resulted in little to no effects on the radiation performance.

Bibliography

[1] National Research Council, Controlling cost growth of NASA Earth and Space Science Missions, Washington, D.C.: National Academies Press, 2010.

[2] D. Kramer, Costs for polar-orbiting weather satellites climb again, Physics Today, vol. 65, no. 8, August 2012

[3] R. Sandau, Status and trends of small satellite missions for Earth observation, Acta Astronautica, vol. 66, nos. 1-2, p. 1-12, January/February 2010

[4] P. Ferguson, Making Space for Everyone: A Research Program Aimed at Breaking Down Barriers to New Technology Adoption in Space, in Proceedings of the CASI/IASC ASTRO, Quebec City, QC, Canada, May 2018

[5] F. Christin, CMC Materials for Space and Aeronautical Applications, in Ceramic Matrix Composites, ed: Wiley-VCH Verlag GmbH & Co. KGaA, 2008, p. 353.384

[6] R. Deo, H.H. Starnes, and R.C. Holzwarth, Low-cost composite materials and structures for air-craft applications, NATO RTO AVT Panel spring symposium and specialists' meeting Loen, Norway, 2001

[7] T. Thompson, C. Grastataro, B. Smith, G. Krumweide and G. Tremblay, Development of an All-Composite Spacecraft Bus for Small Satellite Programs, Proceedings from AIAA/USU Conference on Small Satellites, Utah State University, August 1994.

[8] W. Kinsner, D. Schor, R. Fazel-Darbandi, B. Cade, K. Anderson, C. Friesen, S. McKay, D. Kotelko, P. Ferguson, The T-Sat1 Nanosatellite Design and Implementation Through a Team of Teams, International Journal of Cognitive Informatics and Natural Intelligence, vol. 7, no. 1, July 2015

[9] H. Heidt, P. Jordi, M. Augustus, N. Shinichi, T. Robert, CubeSat: A New Generation of Picosatellite for Education and Industry Low-Cost Space Experimentation, Proceedings from AIAA/USU Conference on Small Satellites, Utah State University, 2000

[10] D. M. Pozar, Microstrip Antennas, in Proceedings of the IEEE, vol. 80, no. 1, p. 79-91, January 1992

[11] M. A. Swartwout, CubeSat Census, [Online]. Available: https://sites.google.com/a/slu.edu/swartwout/home/cubesat-database/census, [Accessed: 16-May-2020]

[12] Bryce Space and Technology, State of the Satellite Industry Report, [Online]. Available: https://brycetech.com/reports/report-documents/Bryce_Smallsats_2020.pdf, [Accessed: 16-May-2020]

[13] Y. Rahmat-Samii, V. Manohar and J. M. Kovitz, For Satellites, Think Small, Dream Big: A review of recent antenna developments for CubeSats, in IEEE Antennas and Propagation Magazine, vol. 59, no. 2, p. 22-30, April 2017

[14] S. Gao et al., Antennas for Modern Small Satellites, in IEEE Antennas and Propagation Magazine, vol. 51, no. 4, p. 40-56, Aug. 2009

[15] C. Balanis, Antenna Theory: Analysis and Design, 3rd ed. Hoboken, NJ: John Wiley, 2005.

[16] F. E. Tubbal, R. Raad and K. Chin, A Survey and Study of Planar Antennas for Pico-Satellites, in IEEE Access, vol. 3, p. 2590-2612, 2015

[17] A. Emmanuel, Design and development of a multifunctional composite radiation shield for space applications, Ph.D. Thesis, University of Manitoba, Winnipeg, Canada, 2016

[18] R. Dybdal, Communication Satellite Antennas: System Architecture, Technology, and Evaluation, 1st ed. McGraw-Hill, 2009

[19] M. C. Vigano, G. Toso, P. Angeletti, I. E. Lager, A. Yarovoy, and D. Caratelli, Sparse Antenna Array for Earth-coverage Satellite Applications, in Proceedings of the Fourth European Conference on Antennas and Propagation, Barcelona, Spain, April 2010

[20] S. K. Rao, Advanced Antenna Technologies for Satellite Communications Payloads, IEEE Transactions on Antennas and Propagation, vol. 63, no. 4, p. 1205–1217, April 2015

[21] D. Isleifson and L. Shafai, Design and Test of a Dual-Frequency Dual-Polarization Microstrip Patch Array Prototype, in Proceedings from 18th International Symposium on Antenna Technology and Applied Electromagnetics (ANTEM), Waterloo, ON, Canada, 2018

[22] Z. L. Hui, Q. Xiao, and L. S. Yang, Review of Large Spacecraft Deployable Membrane Antenna Structures, Chinese Journal of Mechanical Engineering, vol. 30, no. 6, p. 1447–1459, November 2017

[23] I. Singh and D. V. Tripathi, Micro strip patch antenna and its applications: A survey, International Journal of Computer Applications in Technology, vol. 2, no. 5, p. 1595-1599, 2011.

[24] S. Shrestha, M. Agarwal, P. Ghane, and K. Varahramyan, Flexible microstrip antenna for skin contact application, International Journal of Antennas and Propagation, Jun. 2012, Art. ID 745426.

[25] F. Ferrero, C. Luxey, R. Staraj, G. Jacquemod, M. Yedlin, and V. Fusco, A novel quad-polarization agile patch antenna, IEEE Transactions on Antennas and Propagation, vol. 57, no. 5, p. 1563-1567, May 2009.

[26] S. Gao, A. Sambell and S.S. Zhong, Polarization-agile antennas, in IEEE Antennas and Propagation Magazine, vol. 48, no. 3, p. 28-37, June 2006

[27] C.Y. Chiu, K.M. Shum, C.H. Chan, and K.M. Luk, Bandwidth enhancement technique for quarter-wave patch antennas, IEEE Antennas and Wireless Propagation Letters, vol. 2, no. 1, p. 130-132, Feb. 2003.

[28] P. Salonen, M. Keskilammi, and M. Kivikoski, New slot configurations for dual-band planar inverted-F antenna, Microwave and Optical Technology Letters, vol. 28, no. 5, p. 293-298, Mar. 2001.

[29] H. Malekpoor and S. Jam, Enhanced bandwidth of shorted patch antennas using folded-patch techniques, IEEE Antennas Wireless Propagation Letters, vol. 12, p. 198–201, Feb. 2013.

[30] A. Nascetti, E. Pittella, P. Teofilatto, and S. Pisa, High-gain S-band patch antenna system for earth-observation CubeSat satellites, IEEE Antennas Wireless Propagation Letters, vol. 14, p. 434-437, November 2015

[31] R.M. Rodríguez-Osorio and E.F. Ramírez, A Hands-On Education Project: Antenna Design for Inter-CubeSat Communications [Education Column], in IEEE Antennas and Propagation Magazine, vol. 54, no. 5, p. 211-224, October 2012

[32] H. Oraizi and A.R. Sharifi, Design and optimization of broadband asymmetrical multisection wilkinson power divider, IEEE Transactions on Microwave Theory and Techniques, vol. 54, no. 5, p. 2220-2231, May 2006

[33] A. Holub and M. Polivka, A novel microstrip patch antenna miniaturization technique: A meanderly folded shorted-patch antenna, Proceedings from IEEE Conference on Microwave Techniques, Prague, Czech Republic, April 2008

[34] H. Malekpoor and S. Jam, Miniaturised asymmetric E-shaped microstrip patch antenna with folded-patch feed, in IET Microwaves, Antennas and Propagation, vol. 7, no. 2, p. 85-91, January 2013

[35] F. Bilotti, A. Alu and L. Vegni, Design of Miniaturized Metamaterial Patch Antennas With μ-Negative Loading, in IEEE Transactions on Antennas and Propagation, vol. 56, no. 6, p. 1640-1647, June 2008

[36] M. P. Magalhães, M. V. T. Heckler, J. C. M. Mota, A. S. B. Sombra and E. C. Moreira, Design and analysis of microstrip antenna arrays for meteorological nano-satellites for UHF uplink, 2014 International Telecommunications Symposium (ITS), Sao Paulo, 2014

[37] M. T. Islam, M. Cho, M. Samsuzzaman and S. Kibria, Compact Antenna for Small Satellite Applications [Antenna Applications Corner], in IEEE Antennas and Propagation Magazine, vol. 57, no. 2, p. 30-36, April 2015

[38] E. Pittella et al., Reconfigurable S-band patch antenna system for cubesat satellites, in IEEE Aerospace and Electronic Systems Magazine, vol. 31, no. 5, p. 6-13, May 2016

[39] J. Padilla, G. Rosati, A. Ivanov, F. Bongard, S. Vaccaro and J. Mosig, Multi-functional miniaturized slot antenna system for small satellites, Proceedings of the 5th European Conference on Antennas and Propagation (EUCAP), Rome, 2011, p. 2170-2174

[40] T.J. Seidel, A. Galehdar, W.S.T. Rowe, S. John, P.J. Callus, K. Ghorbani, The anisotropic conductivity of unidirectional carbon fiber reinforced polymer laminates and its effect on microstrip antennas, Proceedings of Asia-Pacific Microwave Conference 2010.

[41] C.L. Holloway, S. Member, M.S. Sarto, and M. Johansson, Analyzing Carbon-Fiber Composite Materials With Equivalent-Layer Models, IEEE Transactions on Electromagnetic Compatibility, vol. 47, no. 4, p. 833–844, 2005.

[42] J. Ahamed, M. Joosten, P. Callus, S. John, and C.H. Wang, Ply-interleaving technique for joining hybrid carbon/glass fibre composite materials, Composites Part A: Applied Science and Manufacturing, vol. 84, p. 134–146, January 2016

[43] K. Woellert, P. Ehrenfreund, A.J. Ricco, H. Hertzfeld, Cubesats: Cost-effective science and technology platforms for emerging and developing nations, Advances in Space Research, vol. 47, no. 4, p. 663-684, February 2011

[44] V. Platero, M. Nickel, P. Ferguson, Outreaching for the Stars with ManitobaSat-1: An Educational Program Making Space More Accessible to Elementary Schools, Proceedings of the CASI/IASC ASTRO, Montreal, QC, Canada, June 2019

[45] J. Guerrero, E. Fosness, S. Buckley, Multifunctional Structures, Proceedings from AIAA Space 2001 Conference and Exposition, Albuquerque, NM, August 2001

[46] D.M. Barnett and S. P. Rawal, Multifunctional structures technology experiment on Deep Space 1 Mission, in IEEE Aerospace and Electronic Systems Magazine, vol. 14, no. 1, p. 13-18, January 1999

[47] D.M. Barnett, S.P. Rawal, and K. Rummel, Multifunctional Structures for Advanced Spacecraft, Journal of Spacecraft and Rockets, vol. 38, no. 2, p. 226–230, March/April 2001

[48] G. Aglietti, C. Schwingshackl, and S. Roberts, Multifunctional Structure Technologies for Satellite Applications, The Shock and Vibration Digest, vol. 39, no. 5, p. 381-391, September 2007

[49] K.K. Sairajan, G.S. Aglietti, K.M. Mani, A review of multifunctional structure technology for aerospace applications, Acta Astronautica, vol. 120, p. 30-42, March/April 2016

[50] M. Driedger, et al., Design of a Modular Nanosatellite System for T-SAT3, Proceedings from IAF International Astronautical Congress, Guadalajara, Mexico, September 2016

[51] A. Yahyaabadi et al., ManitobaSat-1: A Novel Approach for Technology Advancement, in IEEE Potentials, vol. 39, no. 4, p. 17-23, July-August 2020

[52] T.S. Jang, D.S. Oh, J.K. Kim, K.I. Kang, W.H. Cha, S.W. Rhee, Development of multi-functional composite structures with embedded electronics for space application, Acta Astronautica, vol. 68, no. 1-2, p. 240–252, January/February 2011

[53] C.L. Moore, Gossamer spacecraft technology for space solar power systems, Proceedings from IEEE Aerospace Conference, Big Sky, MT, USA, August 2002

[54] Y. Lin and H.A. Sodano, Fabrication and Electromechanical Characterization of a Piezoelectric Structural Fiber for Multifunctional Composites, Advanced Functional Materials, vol. 19, no. 4, p. 592-598, February 2009

[55] T. Pereira, Z.H. Guo, S. Nieh, J. Arias, H.T. Hahn, Energy storage structural composites: a review, Journal of Composite Materials, vol. 43, no. 5, p. 549-560, January 2009

[56] S.P. Rawal, D.M. Barnett and D.E. Martin, Thermal management for multifunctional structures, in IEEE Transactions on Advanced Packaging, vol. 22, no. 3, p. 379-383, August 1999

[57] A. Das and M.W. Obal, Revolutionary satellite structural systems technology: a vision for the future, Proceedings from IEEE Aerospace Conference, vol. 2, p. 57-67, Snowmass at Aspen, CO, March 1998

[58] S.E. Hahn, R. Usami, T. Ozaki, Multifunctional structure spacecraft bus technology, Proceedings from the 22nd AIAA International Communications Satellite Systems Conference & Exhibit, Monterey, California, May 2004

[59] A. Cherniaev and I. Telichev, Sacrificial bumpers with high-impedance ceramic coating for orbital debris shielding: A preliminary experimental and numerical study, International Journal of Impact Engineering, vol. 119, p. 45-56, September 2018

[60] J.R. Gaier, W.C. Hardebeck, J.R.T. Bunch, M.L. Davidson, D.B. Beery, Effect of Intercalation in Graphite Epoxy Composites on the Shielding of High Energy Radiations, Journal of Materials Research, vol. 13, no. 8, p. 2297-2301, August 1998

[61] A. Emmanuel, J. Raghavan, R. Harris, and P. Ferguson, A Comparison of radiation shielding effectiveness of materials for highly elliptical orbits, Advances in Space Research, vol. 53, no. 7, p. 1143-1152, January 2014

[62] A. Emmanuel and J. Raghavan, Influence of structure on radiation shielding effectiveness of graphite fiber reinforced polyethylene composite, Advances in Space Research, vol. 56, no. 7, p. 1288–1296, July 2015

[63] M.S. Sharawi, D.N. Aloi, and O.A. Rawashdeh, Design and Implementation of Embedded Printed Antenna Arrays in Small UAV Wing Structures, IEEE Transactions on Antennas and Propagation, vol. 58, no. 8, August 2010

[64] R. Matsuzaki, M. Melnykowycz, and A. Todoroki, Antenna/sensor multifunctional composites for the wireless detection of damage, Composites Science and Technology, vol. 69, no. 15-16, p. 2507-2513, December 2009

[65] R.A. Arenson, Embedding electromagnetic components into CubeSat structures using additive manufacturing, Master's Thesis, The Pennsylvania State University, Pennsylvania, USA, 2017

[66] V. Shirvante, S. Johnson, K. Cason, K. Patankar, N.G. Fitz-Coy, Configuration of 3U CubeSat Structures for Gain Improvement of S-band Antennas, Proceedings from 26th AIAA/USU Conference on Small Satellites, Logan, UT, USA, August 2012

[67] S.M. Baek, M.G. Ko, M.S. Kim, and Y.S. Joo, Structural design of conformal load-bearing array antenna structure (CLAAS), Advanced Composite Materials, vol. 26, no. S1, p. 29-42, March 2017

[68] S.H. Son, S.Y. Eom, and W. Hwang, Development of a smart-skin phased array system with a honeycomb sandwich microstrip antenna, Smart Materials and Structures, vol. 17, no. 3, April 2008

[69] C.S. You and W. Hwang, Design of load-bearing antenna structures by embedding technology of microstrip antenna in composite sandwich structure, Composite Structures, vol. 71, no. 3-4, p. 378-382, December 2005

[70] D. Kim, J. Kim, J. Kim, W.S. Park, and W. Hwang, Design of a Multilayer Composite-Antenna-Structure by Spiral Type, Proceedings in Progress in Electromagnetics Research Symposium Proceedings, Marrakeh, Morocco, p. 1348-1351, March 2011

[71] C.K. Kim, L.M. Lee, H.C. Park, W. Hwang and W.S. Park, Impact damage and antenna performance of conformal load-bearing antenna structures, Smart Materials and Structures, vol. 12, no. 5, p. 672-679, August 2003

[72] J.H. Jeon, W. Hwang, H.C. Park and W.S. Park, Buckling characteristics of smart skin structures, Composite Structures, vol. 63, no. 3-4, p. 427-437, February/March 2004

[73] D.H. Kim, W. Hwang, H.C. Park, and W.S. Park, Fatigue Characteristics of a Surface Antenna Structure Designed for Satellite Communication, Journal of Reinforced Plastics and Composites, vol. 24, no. 1, p. 35-51, January 2005

[74] S. Santapuri and S.E. Bechtel, Nondimensional characterization and asymptotic model development for multifunctional structures with application to load-bearing antennas, Smart Materials and Structures, vol. 23, no. 5, March 2014

[75] R.R. de Assis and I. Bianchi, Analysis of Microstrip Antennas on Carbon Fiber Composite Material, Journal of Microwaves, Optoelectronics and Electromagnetic Applications, vol. 11, no. 1, p. 154-161, June 2012

[76] A. Mehdipour, A.R. Sebak, C.W. Trueman, I.D. Rosca and S.V. Hoa, Performance of microstrip patch antenna on a reinforced carbon fiber composite ground plane, Microwave and Optical Technology Letters, vol. 53, no. 6, p. 1328-1331, March 2011

[77] M. Leininger, F. Thurecht, E. Pfeiffer and A. Ruddle, Advanced grounding methods in the presence of carbon fibre reinforced plastic structures, 2012 ESA Workshop on Aerospace EMC, Venice, Italy, May 2012

[78] N. Ghalichechian and K. Sertel, Permittivity and Loss Characterization of SU-8 Films for mmW and Terahertz Applications, IEEE Antennas and Wireless Propagation Letters, vol. 14, p. 723–726, December 2014

[79] B. Park, E. Afsharipour, D. Chrusch, C. Shafai, D. Andersen and G. Burley, A low voltage and large stroke Lorentz force continuous deformable polymer mirror for wavefront control, Sensors & Actuators A: Physical, vol. 280, p. 197–204, September 2018.

[80] J. Melai, C. Salm, R. Wolters, and J. Schmitz, Qualitative and quantitative characterization of outgassing from SU-8, Microelectronic Engineering, vol. 86, no. 4–6, p. 761–764, 2009.

[81] V. Platero, P. Ferguson, D. Isleifson, 2-in-1 Smart Panels: Embedding Phased Array Patch Antennas within Satellite Structures, 70th International Astronautical Congress, Washington, D.C., October 2019.

[82] V. Platero, P. Ferguson, R. Jayaraman, D. Isleifson, 2-In-1 smart panels: Embedding phased array patch antennas within satellite structures, Acta Astronautica, vol. 175, p. 51-56, October 2020.

[83] European Space Agency, RADARSAT Constellation, Internet: https://earth.esa.int/web/eoportal/satellite-missions/r/rcm, Sept. 16, 2020

[84] Innovation, Science, and Economic Development Canada, Canadian Table of Frequency Allocations (2018 Edition), Internet: https://www.ic.gc.ca/eic/site/smt-gst.nsf/eng/sf10759.html, 2018.

[85] Thales Alenia Space, Integrated S-Band Transponder (ISBT): Multimode in-orbit reconfigurable Communications Transponder datasheet, www.thalesgroup.com/sites/default/files/database/d7/asset/document/isbt_ed4_eng.pdf

[86] Canadian Space Agency. "What is the Canadian CubeSat Project," Internet: http://www.asc-csa.gc.ca/eng/satellites/CubeSat/what-is-the-canadian-CubeSat-project.asp, May 2018.

[87] V. Platero, S. Ramezanzadehyazdi, C. Shafai, D. Isleifson, P. Ferguson, Fabrication of an Embedded Multifunctional Structural Antenna for Spacecraft Applications, 19th International Symposium on Antenna Technology and Applied Electromagnetics 2021. ANTEM 2021, Winnipeg, Canada (Virtual Conference), Aug. 8-11, 2021.

[88] MicroChem, SU-8 2000 Permanent Epoxy Negative Photoresist, SU-8 2075 datasheet, [https://kayakuam.com/wp-content/uploads/2019/09/SU-82000DataSheet2025thru2075Ver4-3.pdf].

[89] D.M. Mattox, Handbook of Physical Vapor Deposition (PVD) Processing, 2nd ed. Amsterdam: Elsevier. Print. 2010.

[90] D. M. Pozar, Microwave Engineering, 4th ed. Hoboken, NJ: John Wiley, 2012.